INTERNATIONAL JOURNAL OF HYDROGEN ENERGY 43 (2018) 7823–7854

Available online at www.sciencedirect.com

ScienceDirect

journal homepage: www.elsevier.com/locate/he

Review Article

Carbon and non-carbon support materials for platinum-based catalysts in fuel cells

Shuaiba Samad [a], Kee Shyuan Loh [a,*], Wai Yin Wong [a], Tian Khoon Lee [a], Jaka Sunarso [b], Seng Tong Chong [c], Wan Ramli Wan Daud [a]

[a] Fuel Cell Institute, Universiti Kebangsaan Malaysia, 43600 Bangi, Selangor, Malaysia
[b] Faculty of Engineering, Computing and Science, Swinburne University of Technology, Jalan Simpang Tiga, 93350 Kuching, Sarawak, Malaysia
[c] College of Engineering, Universiti Tenaga Nasional, Jalan IKRAM-UNITEN, 43000 Kajang, Selangor, Malaysia

ARTICLE INFO

Article history:
Received 23 November 2017
Received in revised form
17 February 2018
Accepted 24 February 2018
Available online 28 March 2018

Keywords:
Fuel cells
Catalyst support
Carbon based
Non-carbon based
Platinum

ABSTRACT

Carbon and other platinum-supporting materials have been studied as electrode catalyst component of low-temperature fuel cells. Platinum (Pt) is commonly used as the catalyst due to its high electro-catalytic activity. Current research is now focusing on using either modified carbon-based or non-carbon-based materials as catalyst supports to enhance the catalytic performance of Pt. In recent years, Pt and Pt-alloy catalysts supported on modified carbon-based and non-carbon-based materials have received remarkable interests due to their significant properties that can contribute to the excellent fuel cell performance. Thus, it is timely to review this topic, focusing on various modified carbon-based supports and their advantages, limitations and future prospects. Non-carbon-based support for Pt and Pt-alloy catalysts will also be discussed. Firstly, this review summarises the progress to date in the development of these catalyst support materials; from carbon black to the widely explored catalyst support, graphene. Secondly, a comparison and discussion of each catalyst support in terms of morphology, electro-catalytic activity, structural characteristics, and its fuel cell performance are emphasized. All the catalyst support materials reviewed are considered to be promising, high-potential candidates that may find commercial value as catalyst support materials for fuel cells. Finally, a brief discussion on cost relating Pt based catalyst for mass production is included.

Contents

Introduction 7824
Carbon catalyst supports 7826
Carbon nanotubes (CNTs) 7826
Diamond 7827

* *Corresponding author.*
E-mail address: ksloh@ukm.edu.my (K.S. Loh).
https://doi.org/10.1016/j.ijhydene.2018.02.154

Graphite 7828
Graphene 7829
Heteroatom-doped carbon supports 7831
Nitrogen-doped CNTs 7832
Nitrogen-doped graphene 7833
Boron-doped graphene 7833
Sulphur-doped graphene 7834
Non-carbon catalyst supports 7834
Silicon carbide (SiC) 7834
Titanium dioxide (TiO_2) 7834
Iridium oxide (IrO_2) 7835
Tungsten oxide (WO_3) 7835
Tin oxide (SnO_2) 7835
Pt nanoparticle sizes and fuel cell performance of modified carbon-based and non-carbon-based support 7837
The high cost of Pt and the advantages of Pt-alloy catalyst 7843
The selling prices of Pt 7843
Alloying Pt-based catalyst with other metals and nitrogen supported carbon and non-carbon materials for the enhancement of fuel cell performance 7844
Conclusion and future perspectives 7846
Acknowledgements 7846
References 7847

Introduction

Carbon 60, or C_{60}, was discovered in 1985 [1] by applying high temperature to graphite. Carbon atoms can bond together in many different arrangements, which are called the allotropes of carbon. Carbon is distinct among all chemical elements in that it can be found in many different forms and with varying micro-textures. The diverse morphologies of carbon make it an attractive material that can be used in a wide range of electrochemical applications. The interaction between a carbon support and platinum (Pt) plays a large role in the electrocatalytic properties of Pt/C. This interaction can be improved by modifying the carbon support surface to form suitable functional groups and better chemical links at the Pt/C interface [2]. To produce an ideal and active electrocatalyst, a carbon support with suitable properties (i.e., high surface area, good crystallinity and high conductivity) should be considered because it can significantly affect the preparation of supported catalysts and the performance of the fuel cells.

According to Antolini (2009) [3], it is very challenging to develop carbon supports with high specific surface area, high electrical conductivity, suitable porosity and high stability in a fuel cell environment. Carbon supports can have a large impact on the electrochemical activities of the fuel cells. Carbon supports should possess a high proportion of mesoporous regions (20–40 nm) to provide a large surface area that is accessible to both the catalyst and the monomeric units of the Nafion ionomer to help excite the diffusion of the chemical species [3]. It has been reported that carbon materials with good crystallinity and high specific surface area can provide the maximum dispersion of Pt nanoparticles and at the same time enhance the electron transfer, which can contribute to better fuel cell performances [3]. In various forms, carbon is thermodynamically stable below 0.2 V and kinetically stable above that potential ($C + 2H_2O \rightarrow CO_2 + 4H^+ + 4e^-$, $E^{\cdot} = 0.207$ V), which means that at higher potentials, carbon tends to be thermodynamically unstable and corrodes easily [4]. However, this limitation can be overcome *via* the oxidation process of carbon itself, which can withstand the high potential applied in fuel cell applications [5].

A catalyst is required to increase the rate of the particular catalytic reaction [6] and Pt is the catalyst material used for both anode and cathode in fuel cells, to catalyse the oxidation and reduction reactions. However, the Pt catalysts are not economically feasible due to low surface areas, therefore, support materials are required to obtain a high dispersion and a narrow distribution of catalyst that can also interact and influence the catalytic activity. The catalyst support materials greatly influence the cost, performance, and durability of polymer electrolyte membrane fuel cells (PEMFCs) and direct methanol fuel cells (DMFCs) [4,7–11]. The durability of the catalyst is also greatly dependent on its support. The requirements for catalyst support materials are (i) high specific surface area (should be greater than 100 $m^2\ g^{-1}$) [12] so that the support materials are able to provide a maximum substrate area for good dispersion of the Pt catalyst nanoparticles; (ii) low combustive reactivity under dry and damp air conditions at low temperatures (<150 °C); (iii) high electrochemical stability when tested in fuel cell conditions; (iv) high proton and electronic conductivity, as a good conductive support material acts as a path that results in better electron transport between the support itself and the catalyst; (v) easily recoverable metal (Pt) in the used catalyst; and (vi) strong interaction between catalyst and the support material, which can influence the electronic nature of the Pt catalysts, thus improving the catalytic properties and enhance the electrocatalyst stability [3,7,13,14]. However,

there are other criteria of a potential support material that should be considered, such as suitable porosity and porous structure, high stability in alkaline and acidic media, compatibility with the electrodes, and the additional water handling capability to prevent flooding in the catalyst layer [15]. Some researchers have suggested that an electrocatalyst support can be made more resistant to corrosion by increasing the catalyst loading relative to the support loading. In such case, the catalyst protects the underlying carbon support from corrosion. It is well known that the carbon black used as a support for PEMFC catalysts is easily oxidized at higher potential (greater than 0.8 V vs. standard hydrogen electrode) and that corrosion of carbon black increases in the presence of Pt nanoparticles. This leads to detachment of Pt from the support and agglomeration of the Pt nanoparticles, as shown in Fig. 1.

Carbon black was among the earliest carbon-based supports used in fuel cell applications. Carbon black has been used extensively due to its low cost, high availability and high mesoporous distribution [2]. Pt and carbon black are the current state-of-the-art catalyst and catalyst-support materials in fuel cells due to their high electro-catalytic activities during fuel cell reactions [16]. The carbon black should be activated before being used as a catalyst support to increase metal dispersion and its catalytic activity. There are two ways to activate the carbon materials, i.e., chemical activation and thermal treatment [3]. Chemical activation, also known as oxidative treatment, can be performed using various oxidants such as nitric acid, hydrogen peroxide or ozone gas. The chemical activation of the carbon surface leads to the loss of basic surface sites and the formation of acidic surface sites [3]. The increasing number of oxygen groups on the carbon support materials enhances the dispersion of the catalyst nanoparticles besides increasing the performance of fuel cells [17]. This is reported by Poh et al. (2008) [18], who proved that smaller nanoparticles of Pt formed on the acid-treated carbon surface relative to the untreated carbon surface. Thermal treatment is performed to remove impurities on the carbon surface. The impurities that usually been removed during thermal treatment are metallic impurities, amorphous carbon, multishell carbon nanocapsules and oxygenated functional groups [19–23]. This impurities removal could help to increase the ECSA of the electrocatalyst (due to the presence of pores, etc.). Thermal treatment is applied to the carbon under inert atmosphere (800–1100 °C) or in air/steam (400–500 °C) [3]. In recent years, modifications of carbon support materials to enhance the interaction and chemical links between the catalyst and the support have received great interest. However, there are a few disadvantages of utilising carbon blacks, such as insufficient electrochemical stability and low catalyst utilisation, that eventually led to the development of new carbon derivatives [19]. Carbon black catalyst supports have the potential to corrode rapidly, especially under transient load and on/off operation conditions [4]. Soo et al. (2015) [16] stressed and highlighted a few issues that might affect the performance despite the significant catalytic activities of Pt supported on carbon black, such as low utilisation of Pt when supported on carbon black, the poisoning of Pt by CO, and the degradation of the catalyst support through a support-corrosion mechanism. Due to those limitations, functionalisations and modifications of carbon and non-carbon supports have been widely explored in recent years to produce highly reactive supports in fuel cell applications.

This review will focus on the recent progress in the researches and developments of catalyst support based on the

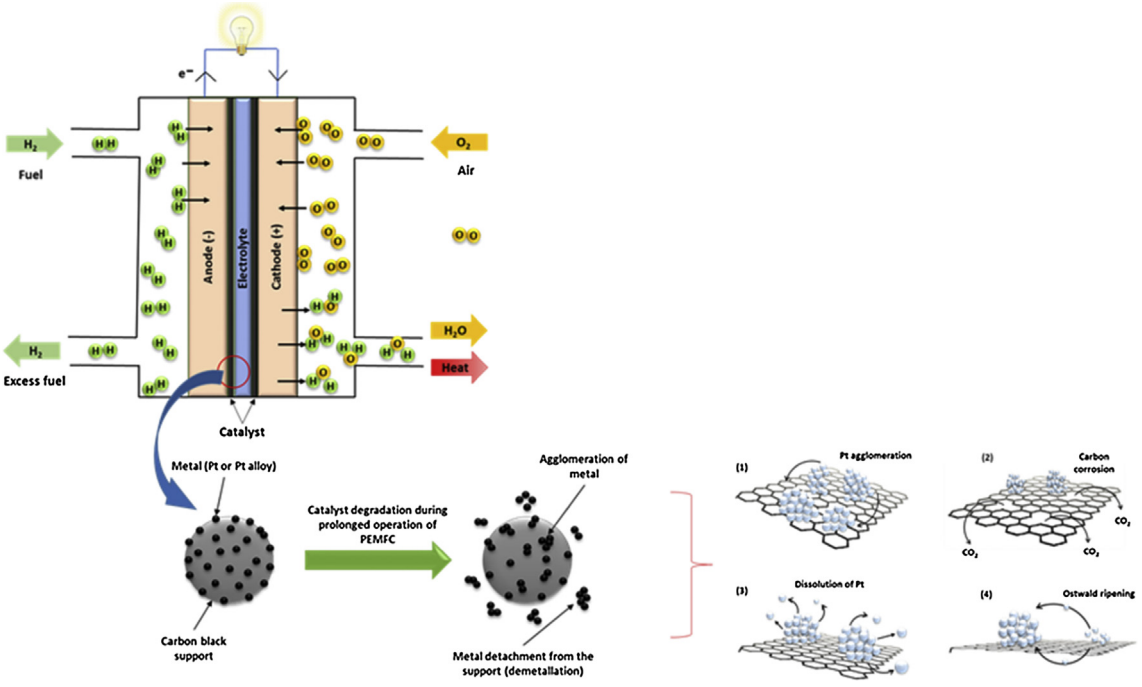

Fig. 1 – Illustration of a typical PEMFC fuel cell with the Pt catalyst on a carbon support and suggested degradation mechanisms of Pt particles on a carbon support in fuel cells.

carbon and non-carbon materials for Pt. Firstly, we shall discuss the variation of catalyst support and its effect towards the catalytic activities, as well as overall fuel cell performances. Secondly, we shall discuss the effect of Pt nanoparticles size, prepared *via* various synthesis route toward the catalytic activity and fuel cell performance. Finally, we shall briefly discuss on the status and cost of the commercially available catalyst and support.

Carbon catalyst supports

Carbon nanotubes (CNTs)

Carbon nanotubes (CNTs) were discovered in 1991 [20], which appears like an elongated version of C_{60}. CNTs consist of cylinders made of graphite layers that are closed at both ends. There are several types of CNTs, i.e., single-walled carbon nanotubes (SWCNTs), which are single graphene sheets rolled into cylinders; double-walled carbon nanotubes (DWNTs); multi-walled carbon nanotubes (MWCNTs) [21], which consist of several co-axially arranged graphene sheets rolled into a cylinder; hollow-structured MWNT/CNFs; bamboo-structured MWNT/CNFs; cup-stacked CNTs (CSCNTs), which have a unique morphology of graphene layers (truncated conical) that grant CSCNTs semiconducting behaviours; herringbone CNFs; and many more. CNTs possess typical characteristics of an outer diameter of 10–50 nm, an inner diameter of approximately 3–15 nm and a length of approximately 10–50 μm [3] that enable them to act as catalyst supports, which is advantageous for a good dispersion of Pt nanoparticles [7]. Commonly, CNTs can be prepared through chemical vapour deposition (CVD) methods because of their low cost and simplicity in preparation [22]. By using this method, Koziol et al. [22] reported that a very high yield of nanotubes could be produced despite the nanotubes' tendency to be structurally malfunctioning in comparison to those produced by arc or laser evaporation methods. Through this method, CNTs are produced from the carbon source, usually in gaseous form, as it decomposes at elevated temperature and passes over a commonly used transition metal catalyst such as iron, cobalt, or nickel.

Briefly, CVD involves the pyrolysis of hydrocarbons (methane, benzene, ethylene, etc.) that are diluted in the stream of inert gas over the surface of the metal catalyst [23]. The catalyst material may be in the form of solid, liquid or gas and can be placed inside the furnace or flowed in continuously from outside [22]. Typical temperatures that are commonly used for the synthesis are in the range of 500–1200 °C [24]. Koziol et al. [22] also reported that the four main parameters for CNT growth in CVD are the atmosphere, carbon source, catalyst, and growth temperature. The researchers mostly preferred to use this method because the products obtained tended to be purer, the growth of the CNTs occurred at a lower temperature, and the metal catalyst can be held on the substrate, which can lead to the growth of aligned nanotubes in a desired direction with respect to the substrate. The advantages of CNTs compared to carbon black are their unique structure that provides high surface area, excellent electrical conductivity, and high chemical stability; resulting in high electrical conductivity and a specific interaction between catalytic metals and the CNT supports. Moreover, CNTs have fewer impurities compared to carbon black that can poison the metal catalyst and are free from deep cracks that lead to low catalytic activity [25]. The tubular form of CNTs makes them absolutely unique among other forms of carbon and allows them to be widely used as an alternative material for catalyst support in heterogeneous catalysis, as reviewed by Antolini (2009) [3].

SWCNTs and MWCNTs as Pt catalyst supports are also capable of enhancing the oxygen reduction reaction (ORR) at both high (150 °C) and normal temperature (60 °C to 80 °C) PEMFCs and DMFCs [26–31]. In Kil et al. (2013) [26], the effect of the addition of MWCNTs to the catalyst layer (CL) on the cell performance (in terms of adhesion strength) was determined by analysing the pore structure and the pore volume of the CL using Pt/C as the metal catalyst. The addition of MWCNTs changed the structure of the pores in the electrodes and increased the volume of the secondary pores. It was also shown that the volume of the primary pores (<100 nm) was not clearly affected by the addition of 10% MWCNTs in the CL; however, when the MWCNT content was further increased, the volume of the primary pores started to decrease. In contrast, the volume of the secondary pores increased when the content of MWCNTs increased. The authors concluded that based on the results obtained, the optimum content of the MWCNT support material for Pt/C in high temperature (150 °C) PEMFC was only 10%, as the highest cell voltage was discovered in the current density region below 0.5 A cm^{-2}. Overly high levels of MWCNTs displayed lower cell voltages, which indicated that MWCNT contents greater than 10% did not produce adequate primary pore volumes for phosphoric acid distribution in CL, which could likely be attributed to the secondary pores having been occupied by the acid. MWCNTs have also been investigated as catalyst supports for single Pt or Pd and bimetal Pt/Au catalysts in various fuel cell applications [27,28,32]. Pt/Au-MWCNT showed a kinetic current density that is 0.7 V higher than that of commercial Pt/C due to the better electronic charge transfer provided by the MWCNT support. Pt/Au-MWCNT also possessed better performance in a single-cell fuel cell test; it was believed that the properties of MWCNTs as a support could ease the transportation of water and gas, allowing the reactants to reach the catalyst sites effectively. MWCNTs can appear in two structures, i.e., bamboo-structured or hollow-structured. Bamboo-structured MWCNTs tend to possess faster electron transfer because the axis of the graphite plane is at an angle to the nanotube, unlike in the hollow structure in which the axis of the graphite plane is parallel to the nanotube axis. The better catalytic activity of electrocatalysts supported by bamboo-structured MWCNTs is aided by the higher percentage of graphitic sheets that terminate at the surface of the tube, which increases the edge plane-like defect sites [7,33,34].

Liu et al. (2015) [35] reported MWCNTs fabricated with silicon nanowires (SiNWs) as a support for an Au metal-based catalyst. Using chemical vapour deposition, silicon nanowire–carbon nanotubes were synthesised. Based on the SEM images, Au formed distinct nanoparticles on the MWNT surfaces with increasing particle sizes when the deposition thickness was increased. At a deposition

thickness of 6.5 nm, the Au nanoparticles appeared to be extended along the axes of the MWNTs; clearly different from the particles formed under 2 and 4 nm thicknesses. The Au nanoparticles showed a highly intermittent structure; indicating weak Au-MWNT interactions and low binding energy. The Au nanoparticle size decreased, with a concomitant decrease in size distribution, when the thickness of the Au layer decreased. For an Au deposition thickness of 2 nm, 77% of the particles obtained were smaller than 11 nm, while for 4 nm thickness, 90% of the particles were in the range of 11–20 nm, and for a deposition thickness of 6.5 nm, 83% of the particles were in the range of 15–50 nm. Liu et al. (2015) [35] concluded that due to the low nucleation density and high diffusion rate, Au atoms consolidated into segregated large particles, while the SiNW morphology could be controlled by adjusting Au layer thicknesses [35]. The thicker Au layers could produce highly active catalysts for SiNW growth and small SiNW diameters.

For CNTs, the diameters and the number of carbon shells generally play a vital role in the performance of the electrocatalyst. SWCNTs usually have diameters in the range of 0.4–3 nm, while MWCNTs are in the range of 1.4–100 nm. Theoretically, in terms of specific surface area, SWCNTs are better than MWCNTs because the smaller the diameter, the higher the surface area, which can provide better dispersion of catalyst nanoparticles. Wu et al. (2007) [36] reported that Pt supported by SWCNTs exhibited better performance for methanol oxidation compared to Pt supported by MWCNTs, not only because of their higher surface area with an abundance of oxygen-containing surface functional groups but also due to their higher graphitic crystallinity to which is attributed the better charge transfer at the electrode and electrolyte interface [36]. However, CNTs without surface modifications displayed lack of binding sites for anchoring precursor metal ions or metal nanoparticles, which can lead to deficient dispersion and agglomeration of metal nanoparticles, especially at high loading conditions [3].

Currently, many researchers are looking towards producing better electrocatalysts with various modifications. One such modification involves nitrogen- or other heteroatom (sulphur, phosphorus)-doped CNTs that are preferable for use as a support for metal catalysts and transition metals (in the form of oxides and carbides) due to their low cost, stability, long-lifetime, high electrical conductivity, and ability to enhance ORR activity [37–41]. Nitrogen itself has an extra electron in the delocalised π orbital of the carbon framework, rendering it a beneficial defect in the structure of carbon materials. Surface defects play a very important role in enhancing the ORR in fuel cells. A higher degree of surface defects can increase ORR activity by exposing more edge-plane nitrogen groups, such as pyridinic and pyrrolic nitrogen, relative to the baseline ORR activity anticipated from their lone pair electrons only [37]. Explorations of other potential metals such as iron, cobalt, or nickel as an alternative better electrocatalysts to Pt are becoming intensive to address the high cost of Pt and the quick decline in the activity of the Pt catalyst [38]. Owing to those circumstances, ongoing research is focusing more on identifying and developing alternative materials that can reduce the cost and at the same time extend the life of fuel cells.

Diamond

Carbon that has a cubic crystal structure in which each atom uses sp^3 bonding to form four strong, covalent bonds is called diamond. The hardness and high melting point of diamond are contributed by these bonds. Diamond has been studied and characterised physically and electrochemically in its powder and thin film forms [42]. Diamond in nano size has been found to be a promising material for a robust and chemically stable catalyst support in fuel cells [43]. Diamond has gained great interest as a catalyst support because of its facile optimisation to achieve desirable attributes, *via* gas-phase chemical vapour deposition, and low-cost fabrication [44]. Additionally, diamond also acquires metal-like conductivity when doped with high concentrations of boron; resulting in an ideal electrode material due to its chemical inertness and corrosion resistance. A few reports have described diamond use as a catalyst support in direct methanol fuel cells, including boron-doped diamond (BDD) powder [45] and p-type silicon/boron-doped diamond (p-Si|BDD) [46].

Recent studies have also shown that BDD could be used as an electrocatalyst support material in fuel cells to improve conductivity, electrochemical stability, and corrosion resistance in an acidic and an alkaline media. BDD in powder form was investigated as a catalyst support for fuel cell applications by Salazar-Banda et al. (2007) [45]. A boron-doped diamond powder modified with metallic oxides *via* a sol-gel method was created to prepare high-surface-area and stable electrodes for the methanol oxidation reaction. Their study showed that the Pt-RuO_x supported on the BDD powder exhibited good electro-catalytic activity towards methanol oxidation (in DMFC) with an onset potential that is 20 mV lower than that of a Pt-Ru/C commercial catalyst. Electrochemical evaluation in an acidic medium has shown that the high purity of the deposited particles allowed a good electrical contact with the diamond powder surface.

Silicon is one of the most common substrates for diamond film studies, as the two materials possess similar properties [44]. Halima et al. (2014) [46] synthesised p-Si|BDD with Pt nanoparticles as the electrocatalyst for the methanol oxidation reduction. The substrate used for the electrode was highly doped metal-like p-Si. This type of Si represents the worst-case scenario in term of its instability with respect to passivation and therefore offers a good basis for rapid corrosion testing. Due to the rapid oxide formation kinetics on degenerate Si, this material is highly suitable for the destructive testing involved. Stability tests were conducted on the p-Si|BDD|Pt by two methods, i.e., (1) long-term aqueous acidic medium exposure (280 h) and (2) continuous cycling between 0 mV and −400 mV in 1 M H_2SO_4. The hydrogen evolution reaction (HER) occurring with an onset potential at −240 mV for the electrode indicated that the Pt coated on the diamond electrode was stable under these conditions. The activation sweep curve was not notably changed after 1000 cycles. Compared to Montilla et al. (2003) [47], a tremendous decrease in current and high instability of the Pt-coated BDD due to dissolution of a significant fraction of the Pt nanoparticles was

observed. The dissolution was caused by the continuous cycling to the oxygen evolution reaction (OER) potential.

Based on the accelerated long-term stability tests, the BDD support was more stable than MWCNTs and the conventional support material Vulcan XC-72 [48]. Moreover, boron has a low charge carrier activation energy of 0.37 V, which make it the most preferable dopant to produce conducting diamond electrodes [49]. The diamond itself is capable of acting as a semimetal or an extrinsic semiconductor, depending on the level of boron doping. With low levels of boron doping, diamond tends to act as an extrinsic semiconductor, while with high levels of boron doping, diamond tends to act as a semimetal [50].

Graphite

Graphite is a crystalline form of carbon and is the most stable form of carbon under standard conditions. It is regarded as a semimetal and is often used to prepare conductive films on electrode substrates because of its excellent intrinsic conductivity [51]. Modifications of the structure of graphite make it capable of functioning as an effective catalyst support for fuel cell applications, typically in PEMFCs [10,52,53] and dye-sensitised solar cells (DSSCs) [54,55]. Graphite materials with different structures such as nanoscale graphite, graphite nanofibres (GNFs), graphite sub-micron particles (GSPs), graphite nanosheets (GNSs), and graphite nanoballs (GNBs) have been examined for their capabilities as potential durable catalyst supports in fuel cells [10,52–54,56–58]. GNFs exhibited increased corrosion resistance over Vulcan XC-72, and the catalytic effect of Pt on GNF corrosion was remarkably decreased compared to that on Vulcan XC-72. GNF support has also shown less Pt surface area loss during continuous cycling in durability tests compared to that of commercial Vulcan XC-72, which demonstrated that GNF is a more durable catalyst support than Vulcan XC-72 in PEMFCs [52].

As mentioned, graphite support materials can be modified to various structures and forms such as nanosheets, nanoballs, nanofibres, nanoscale graphite, crystalline oxides, and sub-micron particles depending on their applications [10,54,56–59]. Schematic illustration of the different carbon structure and the diameters of some modified graphite materials (GNF, GNS and GNB) are shown in Fig. 2.

In Fig. 2(b), the highest diameter is that of GNF (80 nm), followed by GNB (30 nm), and GNS (12 nm). However, from Raman and FTIR results, GNB tends to have the most inner

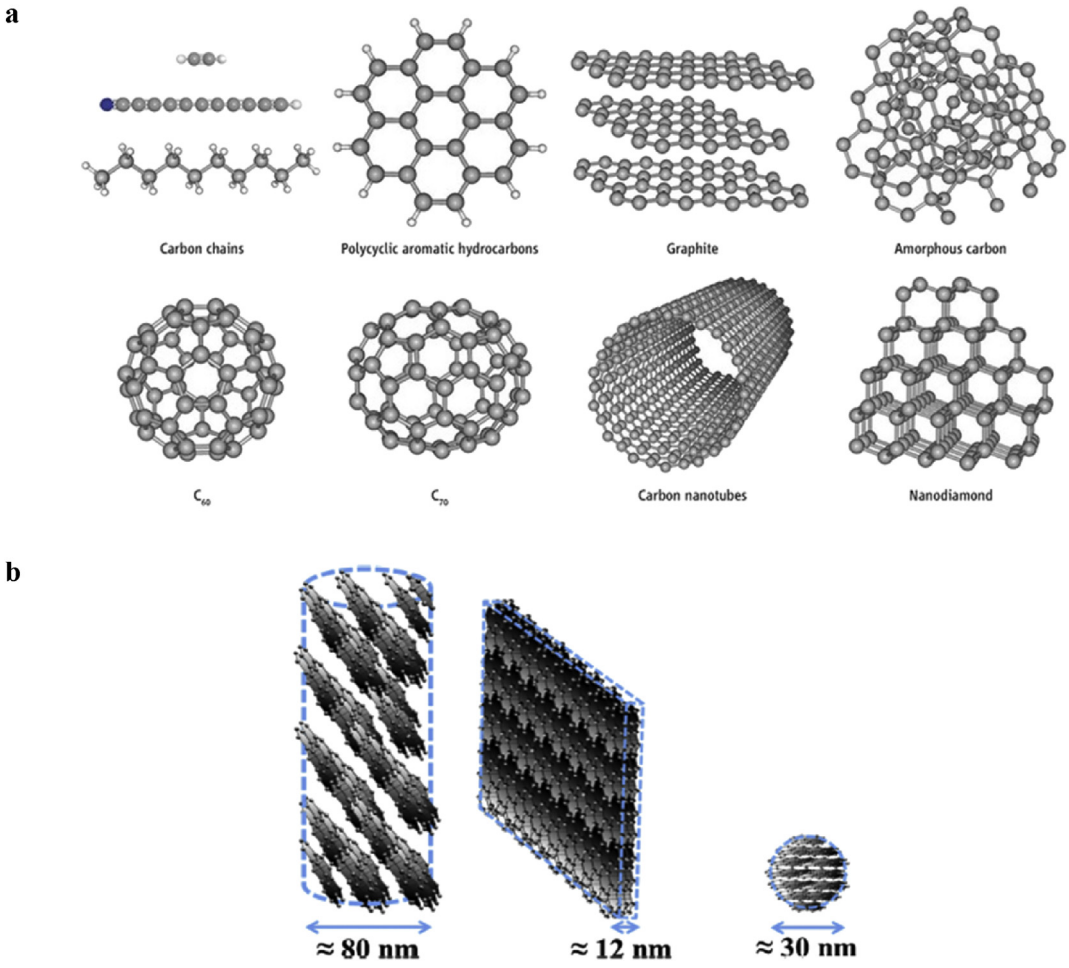

Fig. 2 – Schematic illustration of the (a) different type of carbon structure and (b) diameters of graphite materials (GNF, GNS and GNB). Reproduced with permission [54,301].

defects on the sp^2 planes compared to GNF and GNS, with the presence of edges, vacancies and hydroxyl functional groups on the plane [54]. Defects on carbon support materials enhanced the electron transfer and functioned as electro-catalytic reaction sites [25,33,60–62]. Different graphite structures have been compared as support catalysts in DSSCs. To the best of our knowledge, however, no research has been performed using modified graphite such as GNBs in fuel cell applications. With the most inner defects, the GNB-based DSSC showed the highest power conversion efficiency (η) of 7.88%, while the GNS-based and GNF-based DSSCs showed η values of 2.99% and 3.60%, respectively. Based on the results reported in the literature, the η of the GNB-based DSSC is the closest to the η of the Pt-based (compared to GNF, GNS, and graphite sheet), which is 8.38%. Moreover, cyclic voltammetry and Tafel polarization analysis showed that a GNB counter electrode (CE) possessed the highest values of cathodic peak current density (J_{pc}) at 1.24 mA cm^{-2} compared to GNF and GNS at 1.06 mA cm^{-2} and 0.08 mA cm^{-2}, respectively, along with the highest exchange current density (J_0) of 4.48 mA cm^{-2} compared to GNF and GNS at 0.21 mA cm^{-2} and 0.06 mA cm^{-2}, respectively. The smallest charge transfer (R_{ct}) for electrochemical impedance spectroscopy (EIS) and Tafel polarization analysis of 2.87 Ω cm^2 was obtained on GNB as compared to GNF and GNS, which showed significantly different R_{ct} values of 65.88 Ω cm^2 and 203.60 Ω cm^2, respectively.

Therefore, the electro-catalytic activity of the GNB-based DSSC was higher than those of the other graphite materials, GNF and GNS; demonstrating its potential to replace Pt. It was shown that the inner defects on the sp^2 planes, which in turn determine the electro-catalytic ability of the graphite materials, did not depend on the GNB particle size [54]. According to this study, the power conversion efficiency (η) of a graphite-based DSSC was limited because the active sites of graphite were restricted to the contribution of the edge planes. To overcome this issue, various treatments were applied to increase defects in the structure of graphite, including chemical exfoliation under strongly acidic or toxic environments, because increased levels of defects increases the active sites of the graphite and thus, increases the reaction rate [55,61].

To overcome this limitation of the DSSC performance, the active sites of the GNB should be increased by surface functionalisation with the addition of conductive polymers, as conductive polymers have been proven to exhibit good electro-catalytic performance [63,64]. Examples of the conducting polymers are polyaniline, polyacetylene, polypyrrole and poly(3,4-ethylenedioxythiophene), known as PEDOT, which is a derivative of polythiophene [54,65]. Another method to increase GNB's active sites is by doping with heteroatoms such as nitrogen, boron and sulphur since they are among the most effective and widely used dopants given their similar atomic size to carbon [66,67]. Nitrogen atoms provide an additional lone pair when doped into the graphite open framework that could enhance the process of electron donation from graphite to oxygen, thus increasing the efficiency of oxygen reduction and the electronic properties of the graphite [68–72]. The electron transfer could be further improved when single or multiwall CNTs were added to GNB and could thus enhance the conversion efficiency of the related cell [73].

Another approach using graphite as a catalyst support was studied by Zhang et al. (2010) [10], who proposed low-cost graphite sub-micron particles (GSPs) as a possible long-lasting catalyst support for PEM fuel cells. Pt nanoparticles were deposited on Vulcan XC-72 carbon black, CNTs, and GSPs *via* an ethylene glycol reduction method. The crystallinity and the morphologies were studied, and based on XRD and TEM analysis, the GSPs showed the most highly ordered graphitic structure, which indicates that the GSPs exhibited the highest electrical conductivity [74]. The average diameters of the Pt nanoparticles in the Pt/XC-72, Pt/CNT, and Pt/GSP were very close, i.e., 2.2 nm, 2.3 nm, and 2.2 nm, respectively; as such, these results cannot directly indicate that the lowest diameter Pt nanoparticles would provide the highest electro-catalytic ability. The electrochemical surface area (ESA) of Pt was calculated by coulombic charges accumulated during hydrogen absorption and desorption, and the ESA values were 52.2, 49.5, and 50.2 m^2 g^{-1} Pt for Pt/XC-72, Pt/CNT, and Pt/GSP, respectively. Zhang et al. (2010) [10] also investigated the degraded percentage of the ESA of the catalysts in the durability test under potential steps (1.4–0.85 V) for 22 h. The results showed that the ESA degradation for Pt/XC-72, Pt/CNT, and Pt/GSP was 58%, 47%, and 32%, respectively. The higher stability of the GSP support due to its unique morphology and high crystallinity granted Pt/GSP higher durability, which contributed to higher corrosion resistance.

Based on the reports above, various modifications and functionalized graphite materials have been studied and explored for use as catalyst supports in fuel cell applications. In summary, a few important criteria must be considered to allow the graphite support to exhibit excellent electro-catalytic activity in fuel cell applications. For instance, a higher surface area of the graphite materials along with more defects can increase the durability of the electrode along with the catalytic sites for the reaction in fuel cells. However, the authors felt that the study of different forms of graphite as catalyst supports was critical and worth exploring.

Graphene

Graphene is a two-dimensional (2D), one-atom-thick planar flat sheet of sp^2 tightly bonded carbon atoms with a thickness of 0.34 nm. It is considered to be the fundamental foundation (basic block) for all fullerene allotropes [75]. It is the thinnest and strongest material ever discovered [76]. Graphene can be reshaped into a few forms, i.e., wrapped into zero-dimensional (0D) spherical buckyballs, rolled into one-dimensional (1D) CNTs, or stacked into three-dimensional (3D) graphite [75]. Graphene has the potential to act as a support for both metals [77–82] and non-metals [77,83–85] due to its high surface area [86], which is required to achieve high metal nanoparticle dispersion [3]; good thermal properties [87,88] and high electrical conductivity [89]. Graphene can also be modified chemically or structurally to alter its functionality and hence contribute to its potential applications, such as use in fuel cells, energy storage or generation, electrochemistry, supercapacitors, and batteries [90–92]. Fig. 3 depicts an illustration of the synthetic route used to obtain the graphene nanosheets (GNSs), while Fig. 4 shows their SEM images [93].

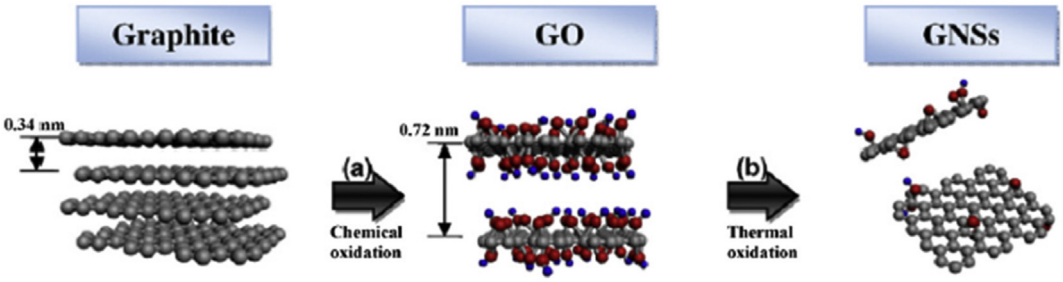

Fig. 3 – Illustration of the synthetic route used to obtain GNSs. Reproduced with permission [93].

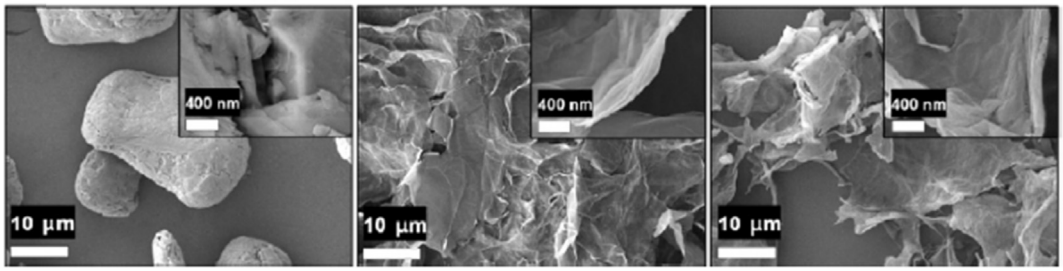

Fig. 4 – SEM images of conversion graphite to GNSs *via* the processes of chemical oxidation and thermal oxidation (exfoliation). Reproduced with permission [93].

The first graphene sheets were discovered in 2004 by mechanically extracting monolayer sheets from the 3D graphite [94]. Graphene can be synthesised using several methods such as chemical vapour deposition [95], solvothermal synthesis with pyrolysis [96], chemical reduction [36] and electrochemical methods [97]. Those are the synthesis methods of graphene without the formation of graphite oxide (GO), Stankovich et al., 2007 [36] decided to prepare GO as an intermediate to synthesise graphene sheets. However, the most common, easy, rapid, and low-cost method that is widely used is the oxidation of graphite to graphene oxide using a strong oxidising agent and strong mineral acid, followed by exfoliation in water and reduction of GO to GNS using strong reducing agents. Reduction is the most important step in synthesising graphene sheets as it removes the oxygen functional group from GO and restores the electrical properties of the synthesised graphene [36]. During the reduction process, the brown dispersion of GO turned black, started to agglomerate, and finally produced a precipitate, which indicated that the reduced GO (r-GO) had become less hydrophilic due to the removal of the oxygen functional groups [36,98]. In the same study by Stankovich et al. (2007) [36], they found that the best reducing agent to produce very thin graphene was hydrazine hydrate ($H_2NNH_2 \cdot H_2O$). The r-GO had a significant increase in carbon/oxygen (C/O) atomic ratio to 10.3 compared to that of the GO precursor, which was only 2.7; proving that hydrazine hydrate was highly effective in removing oxygen functional groups [98].

Li et al. (2009) [99] reported a route to synthesise Pt/graphene nanocomposites using reduction in a one-pot method of graphite oxide and chloroplatinic acid that has opened new approaches to study the use of graphene-supported Pt catalysts for low-temperature fuel cells. The development of graphene for use as a catalyst support for Pt catalyst has been explored recently by numerous researchers because it has high stability and electro-catalytic ability and, most importantly, allows high catalyst loading [100]. Graphene-supported Pt has received wide attention as an electrocatalyst in fuel cells, especially PEMFCs, due to its lower cost (relative to Pt) and strong performance [9,101,102]. A study on the effects of adding carbon black to the graphene sheets found that it enhanced the mass transport and at the same time increased the availability of Pt nanoparticles for the electrochemical reactions in fuel cells [101,102]. The addition of carbon black as a spacer between graphene sheets could increase the Pt consumption. This has improved the effectiveness of Pt nanoparticle utilisation for the electrochemical reactions in fuel cells, because the existence of the spacer could trigger the disruption of the horizontally stacked graphene sheets and make them disperse in the catalyst layer randomly [77]. On the other hand, Yoo et al. (2009) and Cheng et al. (2014) [9,103] focused on the characterisation of graphene as a catalyst support in the form of nanosheets. Yoo et al. (2009) [103], reported that graphene nanosheet-supported Pt (Pt/GNS) exhibits higher catalytic activity compared to Pt/C due to the maximum vacancies of carbon and defects in GNS that cause Pt clusters to interact strongly with GNS and Pt particles. Cheng et al. (2014) [9], who studied GNS with pores, found that it has greatly enhanced electrochemical activities because the pores can increase the mass diffusion speed and contribute to the increase in the rate of reaction (in terms of diffusion of species). Fig. 5 shows the schematic of the reactive process at the cathode in PEMFC; (a) dispersion of Pt nanoparticles on graphene sheets (b) the transfer of reactive species is only through the edges of the GNS and (c) the transfer of reactive species is more ease through the pores in GNS. In addition, the ESA analysis showed that Pt-supporting porous GNS exhibited

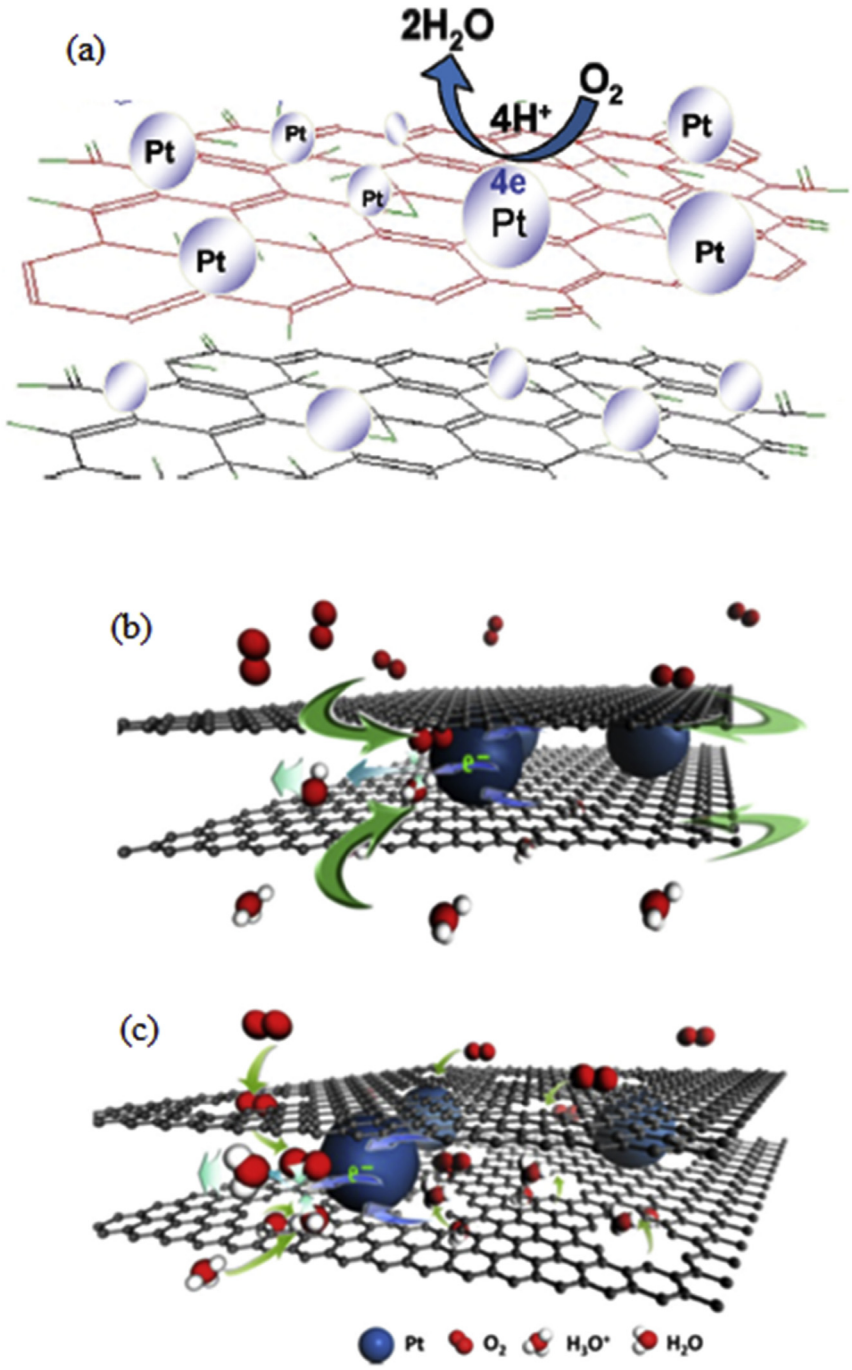

Fig. 5 – (a) Dispersion of Pt nanoparticles on graphene sheets (b) the transfer of reactive species is only through the edges of the GNS; (c) the transfer of reactive species is more ease through the pores in GNS. Reproduced with permission [9,104].

higher value (74.4 $m^2 g^{-1}$) than Pt-supporting GNS (64.7 $m^2 g^{-1}$) and Pt-supporting carbon black (61.2 $m^2 g^{-1}$).

Literature reports reveal that graphene has received such great interest among researchers recently due to its superior physical and chemical properties, which could contribute to high performance of electro-catalytic activities in fuel cell applications. It has strong potential to support either metal or non-metal catalysts, and further studies should explore how graphene could be used to enhance or trigger the best performance in fuel cells.

Heteroatom-doped carbon supports

Modifications of either carbon-based or non-carbon-based supports clearly lead to higher specific surface area and higher electronic conductivity that can definitely enhance fuel cells performance, especially in alkaline media. However, the activity of the carbon catalyst support could be enhanced to a greater extent by doping with heteroatoms such as nitrogen, sulphur, boron, which has been intensely studied [37,83,105–110]. These functional groups could modify the

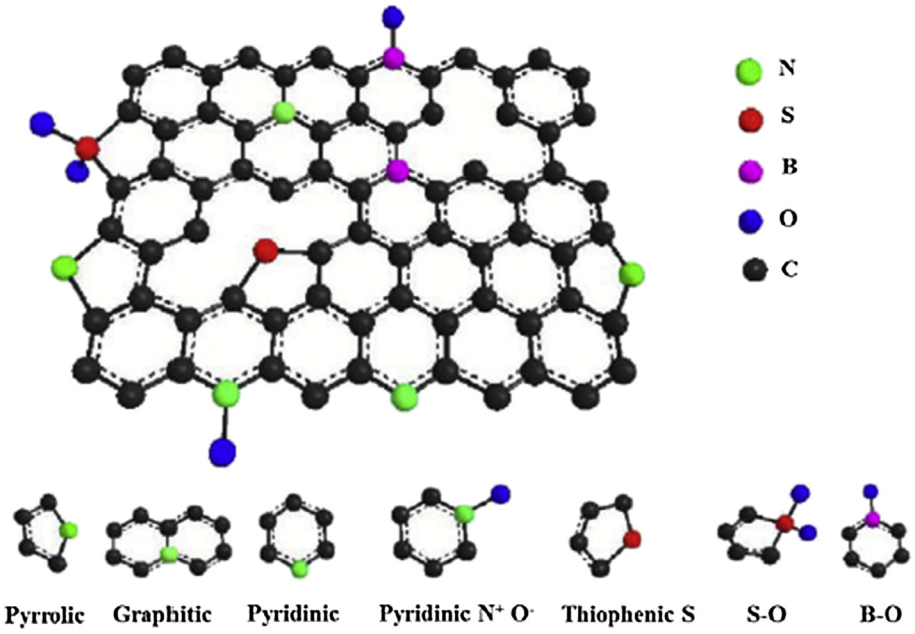

Fig. 6 – Schematic illustration of heteroatoms doped graphene. Reproduced with permission [111].

nucleation and kinetics growth during the dispersion of metal catalyst nanoparticles to provide more homogeneous distribution and smaller size of catalyst nanoparticles; modify the electronic structure of the metal nanoparticles resulting in better intrinsic catalytic activity; enhance the metal-support interaction/chemical binding to provide higher durability [105]. Fig. 6 shows the schematic illustration of various heteroatoms doped on graphene sheets.

Nitrogen-doped CNTs

The doping of CNTs with heteroatoms has been intensively investigated over the recent years because the doping was proven to enable the tuning of both physical and chemical properties of the CNTs that modify their electronic structure [67,83]. Nitrogen is the most widely used heteroatom because of its large electronegativity value (3.04) in comparison with C (2.55) [112]. Nitrogen atoms provide additional lone pairs of electrons when incorporated into a carbon network that could facilitate the electron transfer process from carbon to oxygen which can enhance the electronic properties of the carbon materials that lead to enhanced ORR activity and this was proven based on model simulations by Strelko et al. [37,67–69]. There are two methods to dope the N into CNTs which can be divided into two; (i) "in-situ" doping (direct doping) and (ii) post doping (post-treatment of CNTs with N precursors such as nitrogen gas, ammonia gas, etc.) [67,113]. The "in-situ" doping method is the most common method to synthesis N-CNTs [114]. "In-situ" doping method can be categorised into two; (i) high temperature synthesis method and (ii) low temperature synthesis method [114]. High temperature synthesis method includes arc-discharge and laser ablation [115–119]. Low temperature synthesis method includes CVD [37,109] and other modified CVD methods (floating catalyst CVD [120], plasma enhanced CVD [121,122], pyrolysis-type CVD [123] and aerosol assisted CVD [124]).

Chen et al. (2009) [125] studied on the electrochemical stabilities of Pt/CNTs and Pt/NCNTs with different nitrogen contents and melamine (200 mg, 800 mg and 2000 mg). Pt nanoparticles were deposited on the CNTs and NCNTs using ethylene glycol reduction method. The increment of nitrogen contents caused the Pt nanoparticles sizes to decrease which provide higher specific surface area for the reaction to take place. The well-dispersed of Pt nanoparticles on NCNTs can be attributed to the defects on the surface structure, enhanced wettability and increase of surface active sites by the N doping [126]. Chen et al. (2009) [125] also studied the reactivity of the Pt/CNTs and Pt/NCNTs by evaluating the electrochemical surface area (ESA). After 4000 voltammetric cycles, only 20.2% of the initial ESA of Pt/NCNTs (1.5 at% N) remained, and as the nitrogen content increased, the remaining initial ESA also increased 26.6% and 42.5% for Pt/NCNTs 5.4 at% N and 8.4 at% N, respectively. Thus, indicating that the stability increases when the nitrogen content increases.

Sharing the same objectives, Guo et al. (2015) [127] also studied on the Pt supported N-doped CNTs (Pt/NCNTs). They investigated on how the embedding of Pt nanoparticles into the NCNTs could be done efficiently by using in situ reduction method (heat treatment). Guo et al. (2015) found out that the NCNTs provided the pathway in for the electrolyte to reach the Pt surface and at the same time retained the better electron transfer of CNT by evading the damage of structure of the CNTs. Moreover, NCNTs play a big role by preventing the Pt nanoparticles from agglomerations, dissolutions and migrations during accelerated durability test (ADT) or during heat-treatment process [127]. The addition of NCNTs as support to Pt catalyst showed significantly increased cathodic current density and enhanced sensitivity towards ORR, specifying

that oxygen can efficiently reach the Pt nanoparticles surfaces [127].

Nitrogen-doped graphene

Nitrogen-doped graphene is another popular carbon material doped with heteroatom N, acts as an efficient catalyst and catalyst support in fuel cell applications. Possessing indistinguishable properties to CNTs including structure, good electronic states and good mechanical properties, graphene is an appealing candidate for an efficient catalyst support where the CNTs have been exploited [128]. Moreover, the 2D structure of graphene could facilitate the transfer of electron [129]. When an N atom is incorporated into graphene network, it usually has three common bonding configurations within the carbon lattice; pyridinic N, pyrrolic N and graphitic N (or known as quaternary N) [84]. Briefly, pyridinic N (sp^2 hybridised) bonds with two carbon atoms at the edges of the graphene (defects) and donates one p electron to the π system. Unlike pyrrolic N (sp^3 hybridised) which the N atoms donate two p electrons to the π system. Graphitic N (sp^2 hybridised) refers to N atoms that replace the C atoms in the hexagonal ring [84,113,130]. Nitrogen-doped graphene can be synthesised by using a few methods such as CVD [128,131], thermal treatment [132–134] and plasma treatment [135,136].

Pt supported nitrogen-doped graphene has been widely studied due to the excellent properties of the graphene itself and the N-doping that could greatly enhance the durability and the catalytic activity of the Pt catalyst [90,125,137]. Jafri et al. (2010) [135] investigated the performance of Pt catalyst supported graphene (Pt/G) and Pt catalyst supported nitrogen-doped graphene (Pt/NG) for ORR in PEMFC. The Pt/NG was synthesised by using nitrogen plasma treatment which created pyrrolic N defects (sp^3 hybridised) that could provide good anchoring sites for the Pt nanoparticles deposition. The MEA fabricated with Pt/NG as the ORR catalyst showed a maximum power density of 440 mW cm^{-2} which is higher than Pt/G (390 mW cm^{-2}). The performance enhancement in Pt/NG as the ORR catalyst was attributed to the efficient Pt-carbon binding and the improved electrical conductivity due to the N-doping [135]. Besides the N defects, the O defects in the surface of graphene that appeared due to the exfoliation of graphite also could act as the anchoring sites for the better Pt nanoparticles deposition. Not only that, the doping of nitrogen could also increase the binding energy of Pt nanoparticles to the substrate. The binding energy gets stronger when there are more N atoms that are closer to the C atoms which bond directly to the Pt particles [135,138]. The doping of nitrogen with carbon materials was also capable to decompose reactive intermediates such as H_2O_2 to O_2 during the ORR [139].

Jafri et al. (2015) [79] further studied on Pt/NG using two different methods; hydrothermal method (Pt/NG) and thermal solid state method (Pt/NGA) for ORR in PEMFC and also for MOR. In both catalysts, MWCNTs were added as spacer to prevent the agglomerations of the graphene sheets. The adding of MWCNTs not only improved the utilisation of catalytic Pt sites, but also the catalyst layer with nice coating can be attained because MWCNTs have good dispersion in water and this was proven by the MEA results. The MEA results of Pt/NG and Pt/NGA showed the maximum power density of 366 mW cm^{-2} and 328 mW cm^{-2}, respectively. When MWCNTs were added to the Pt catalysts, the maximum power density increased to 704 mW cm^{-2} and 650 mW cm^{-2}, respectively.

The N-doping with graphene is not only being explored as catalyst and catalyst support for PEMFCs but also other applications such as DMFCs [140,141], lithium battery [142,143] and biosensors [144,145]. The wide interest was gained because the larger surface area of graphene and the N-doping showed a much better catalytic activity, long term operation stability and tolerance to crossover and poison effects than the commercial Pt/C [128]. Besides, the study of the N-doped graphene to support the Pt catalyst could lower the cost as the loading of the Pt will be reduced instead of Pt catalyst without any carbon support and heteroatom doping. It is clearly proven that doping carbon materials with heteroatom N was able to produce an active electrocatalyst for fuel cell applications. More active catalysts could reduce the generation of H_2O_2 by producing water as by-products from the reduction of oxygen doped-carbon surface by a four-electron pathway.

Boron-doped graphene

Heteroatom boron (B) is another element that is being used widely as a dopant to carbon materials for various applications, mainly in fuel cells due to its similar properties as the nitrogen, because the difference of valence electron of boron and nitrogen is only one compared to carbon [146]. The difference causes the emergence of valence band when the position of C atoms in the graphene network localized states below the Fermi level were substituted with boron atoms [147]. This initiates the ability of carbon to react with donor-type molecules (boron) and could be pondered as p-type conductor because of the localized states that caused by the appearance of holes in the structure [146]. Moreover, B-doping retains the planar form of the graphene which has high specific surface area and good for the Pt nanoparticles dispersion.

Thermal annealing, sodium borohydride reduction, polyol and modified polyol methods are among the common methods used to synthesis Pt supported on B-doped graphene (Pt/BG) [148,149]. Sun et al. (2015) [148] reported on Pt/BG and its performance towards methanol electro-oxidation reaction. They found out that Pt/BG exhibits higher peak current density compared to Pt/G and Pt/C, indicating that Pt/BG undergoes better MOR activity. This is because the d-band center of Pt was lowered due to the enhanced electronic interaction between Pt nanoparticles and the BG thereby reducing the adsorption of carbon monoxide (poisoning active intermediate by-product). The formation and the strong adsorption of carbon monoxide (CO) will block the active sites of the catalyst thus affecting the MOR to be very slow [150]. Sun et al. (2015) conducted CO stripping experiment in order to investigate the reason of the enhanced MOR activity of Pt/BG. The results show negatively shifted of peak potential and onset potential of Pt/BG and Pt/G by 60 mV and 23 mV, respectively, which indicate that the oxidation of adsorbed CO occurred more easily on catalyst Pt/BG compared to Pt/G [148]. Therefore, they concluded that the excellent tolerance of CO contributes to the excellent MOR activity of Pt/BG. The oxidation of the adsorbed

CO is further studied through XPS analysis. XPS results revealed that the percentage of oxygen of Pt/BG is lower than Pt/G which is 8.7% and 9.1%, respectively. It is widely stated that the CO oxidation increases due to low strength of CO absorption and more oxygen functional groups [148]. However, the XPS results did not support that the high CO oxidation on Pt/BG is attributed to more oxygen functional groups.

A few other ideas on the influence of B-doped graphene have been discussed, one of the most interesting studies is Pullamsetty et al. (2015), who investigated the Pt/BG through different reduction methods (sodium borohydride reduction, polyol and modified polyol method). They found out that modified polyol method is a competent method to synthesis Pt nanoparticles on the BG with less agglomeration, highly well dispersed and optimum nanoparticles sizes and hence give the best performance compared to Pt/BG.

Sulphur-doped graphene

Sulphur-doped carbon materials are infrequently investigated because the successful incorporation of S atoms to carbon matrix is still a big challenge [151]. S-doping is more difficult to happen compared to N-doping because of the sulphur atomic size and its different binding behaviour [152]. There are a few successful approaches of S-doping such as thermal annealing [153,154] and CVD [155] to intrinsically embed the S atom into the carbon matrix. Yang et al. (2012) reported that S-doping graphene can occur when annealing process was carried out at 500 °C – 1000 °C to form thiophene-like S and oxidized S either at the edges or on the plane of the graphene [151]. Dai et al. (2009) [156] reported that S-doped graphene and B-doped graphene have similar O_2 adsorption energy, thus theoretically S-doped graphene could exhibit good catalytic activity as B-doped graphene [157]. To the best of our knowledge, reports on S-doped graphene as support to Pt catalyst are very few and countable [158–161].

Wang et al. (2013) [160], Park et al. (2014) [158] and Higgins et al. (2014) [159] are among the three latest reports on S-doped graphene as support to Pt catalyst (using three different synthesis methods; formic acid preparation technique, thermal treatment and modified ethylene glycol technique, respectively) for ORR in fuel cell application. The three reports revealed that the Pt supported S-doped graphene (Pt/SG) could increase the catalytic activity with higher limiting current density and higher durability compared to Pt/G and Pt/C.

Generally, sulphur acts as an electron donor and compared to N-doping and B-doping, S-doping displays varying changes at the electronic density of states [146]. The existence of the lone pair electrons could enhance the local reactivity of S-doped graphene. Sulphur (100 p.m.) has larger radius than C (70 p.m.) compared to N (65 p.m.) and B (85 p.m.) that makes the substitution of S into sp^2 lattice difficult because the planar structure will be distorted. Denis et al. (2009, 2011, 2013) [162–164] scrutinized this issue thoroughly and presented the substantial findings regarding the S-doped graphene. They mentioned that the S-doping is possible because it modifies the electronic structure of the graphene (but depends on the S content). They further studied that the S content influences the band gap, as graphene has zero-band-gap semiconductor behaviour, *via* S-doping, the band gap can be opened thus it enhanced the electronic properties.

Non-carbon catalyst supports

Silicon carbide (SiC)

Silicon is a widely used as non-carbon support in various applications such as fuel cells (i.e., PEMFCs) and sensors [11,165,166]. However, the relatively low electronic conductivity of Si hinders its commercial application. One significant approach has been the addition of carbon into silicon carbide (SiC) that acted as an electron conductor to boost the electronic conductivity [165,167]. SiC has been found to be a unique catalyst support due to its high specific capacity, low discharge voltage and good resistance to electrochemical oxidation [165,168,169].

Lv et al. (2010) [165] used SiC as an electrocatalyst support. Using an ethylene glycol reduction method, a dispersion of Pt nanoparticles was deposited on β-SiC (Pt/SiC). SiC showed no change in the redox reaction region after oxidation treatment for 48 h; proving that there were insignificant surface oxides. However, under the same oxidation, a clear change was observed on Vulcan XC-72, where visible current peaks appeared in the redox reaction region resulting from the formation of surface oxides. This verified that SiC was more resistant to electrochemical oxidation than Vulcan XC-72. The electrochemical properties of catalysts were also evaluated in their study. Pt/SiC displayed significant hydrogen and oxygen adsorption and desorption peaks, with no additional current peak observed. These results demonstrated that the SiC support was electrochemically inert and could act as a conductor in the PEMFC electrodes [170]. However, low ESA values revealed that Pt/SiC cannot stand on its own to provide high performance in fuel cells. Si/C itself has low electrical and thermal conductivity, which would diminish the catalytic ability of the Pt catalyst [165,169,171]. Furthermore, based on the ADT, Lv et al., 2010 [165] discovered that the low electrical conductivity of Pt/SiC was caused by a silicon oxide insulator layer that covered the SiC surface.

To overcome this limitation, carbon (Vulcan XC-72) was added into the Pt/SiC catalyst (Pt/SiC/C) to enhance its electrocatalytic performance. The activities of the Pt/C and Pt/SiC/C were compared. For the Pt/C catalyst, Pt particles agglomerated on the carbon supports after the ADT, caused to a decrease in Pt particles on the support, an increase in bare carbon surfaces and an increase in the average particle size from 3 to 8 nm. In contrast, only slight agglomeration of Pt particles was observed on Pt/SiC/C with the average particle size increased to a lower extend, from 3 to 6 nm. The slower agglomeration of Pt particles on Pt/SiC/C demonstrated its higher electrochemical stability compared to Pt/C [165].

Titanium dioxide (TiO_2)

In addition to silicon, TiO_2 has also been investigated as a catalyst support in fuel cell electrodes, especially PEMFCs [4,167,171], given its high stability in an acidic and an aqueous media [167]. However, the same limitation in SiC was also observed in bulk TiO_2, where these non-carbon supports are expected to possess low electro-catalytic activity due to their relatively low electrical conductivity. The important criteria

for good oxide catalyst support are high bulk and surface structural and electronic stability and high bulk and surface electronic conductivity. TiO_2 however is not electrically conducting [4]. To overcome this limitation, various approaches have been attempted such as the addition of carbon materials and cations to TiO_2 [4,167,172].

In work by Kraemer et al. (2008) [167], based on TEM results, demonstrated that the added carbon formed quite homogeneous mixture with Pt/TiO_2 aggregates, despite a small portion of isolated carbon. This was shown to enhance the local electronic conductivity and increase the cell performance remarkably to a level comparable to that of a Pt/C catalyst. This can be attributed to the increase in direct contact between Pt and carbon during the addition of carbon to Pt/TiO_2. Interestingly, the addition of carbon to Pt/TiO_2 resulted in higher thermal stability when tested at 170 °C and 210 °C for 41 days 16 h and 166 days 16 h, respectively, in comparison to Pt/Vulcan XC-72. The latter showed higher degradation rate when tested in the same conditions. Fig. 7 shows the comparison of TEM results of Pt/TiO_2/C with varied Pt to Ti atomic ratios. The samples of (2:1) Pt/TiO_2/C-750 showed the highest ECSA. It is believed that the ECSA for Pt would increase with the increase of TiO_2 content due to the decrease-particle-size effect [173]. However, the lower ECSA of (1:1) Pt/TiO_2/C-750 compared to (2:1) Pt/TiO_2/C-750 might be due to higher quantity of TiO_2 that enclosed the active sites of Pt nanoparticles [173]. In addition to the addition of carbon materials, cations such as tungsten (W) and ruthenium (Ru) have also been used as modifications in Pt/TiO_2 to produce nanoparticles with the required porosity and high surface area to enhance its conductivity and thus increase the performance of the fuel cell [4,172].

Iridium oxide (IrO_2)

Iridium oxide (IrO_2) is another non-carbon catalyst support that gained a good interest among researchers as it is widely known to have high stability corrosion tolerance, outstanding electronic conductivity properties and good stability at high anodic potential [174–176]. However, due to high cost of the Ir and the short electrode lifetime, the use of pure IrO_2 is restricted that caused the expansion of a mixed oxides on the basis of the cheaper and more electrochemically stable carrier oxide containing Ir is clearly hindered [174,177]. One of the roles adding IrO_2 or other mixed oxides such as TiO_2, SiO_2, SnO_2 and etc. to Pt catalyst is to allow the reduction of Pt catalyst in the electrode without a remarkable decline in the catalytic activity and electronic conductivity [174]. Studies on Pt supported IrO_2 have been presented by a few researchers, mainly in Unitized Regenerative Fuel Cells (URFC) [178–180]. Pt/IrO_2 tends to possess poor interdispersion and low bifunctional catalytic activity because of the dispersion of Pt/IrO_2 in the solvent and was found out to be weak [174]. Pt/IrO_2 was usually being used as catalyst for ORR and oxygen evolution reaction (OER). Basically, ORR is the measurement of the current density normalized by the Pt mass while the OER is the measurement of the current density normalized by the catalyst mass [174].

Escalante-Gracia et al. (2010) discovered that Pt/IrO_2 exhibited lower ORR activity but higher overpotential towards OER. However, Pt/IrO_2 is recognized as the most efficient metal oxide for OER in URFC due to its long-term stability to corrosion and it is noticed that the electrocatalytic activity of Pt towards ORR is not affected by the presence of the metal oxide (IrO_2) [179]. The lower ORR activity of Pt/IrO_2 might be attributed to their low conductivity because of the agglomerations of IrO_2 that contain higher ohmic resistance thus inhibiting the electronic pathways between the Pt nanoparticles [174]. This poor conductivity could still be detected although the noble metals loading is increased. To overcome this limitation, one effective approach has been developed to increase the conductivity of the non-carbon support IrO_2, that is adding Ir nanoparticles to the IrO_2 [181,182].

Kong et al. (2012) [181] presented the preparation of Pt supported on $Ir_x(IrO_2)10_{-x}$ by using Adams fusion method. The Pt/$Ir_3(IrO_2)10_7$ catalyst displayed the highest ECSA (24.74 m^2 g^{-1}), the highest ORR activity (21.71 mA mg^{-1} at 0.85 V) and the enhanced OER activity (42.35 mA mg^{-1} at 1.55 V). The improved performance of the Pt/$Ir_3(IrO_2)10_7$ catalyst was obviously contributed by the incorporation of Ir into IrO_2 that increase the electronic conductivity. By using a microwave-assisted polyol method, Ir nanoparticles could also be deposited successfully on the surface of IrO_2 [182]. As expected, the Pt/Ir-IrO_2 exhibited higher ORR activity compared to Pt/IrO_2, and their OER activities were comparable. The enhanced performance of Pt/Ir-IrO_2 was not only due to the increased electronic conductivity, but also ascribed to the interaction between Pt nanoparticles and Ir nanoparticles that prevent the agglomeration of Pt (increase stability of Pt) [182].

Tungsten oxide (WO_3)

Tungsten oxide (WO_3) or also known as tungsten trioxide is an n-type semiconductor with a wide band gap of 2.5–3.2 eV [183,184]. Tungsten has several oxidation states, usually 0 to +6, and it tends to appear in various forms, thereby making it compatible with different applications. WO_3 is water soluble and thermally stable, and due to its distinctive physicochemical properties, WO_3 has gained interest to be applied as catalyst support in fuel cell applications recently. Pt supported on WO_3 has been studied by Chhina et al. (2007) for PEMFC [185]. The study discovered that Pt/WO_3 exhibited higher stability in acidic medium for ORR compared to that Pt/XC-72. Although Pt/WO_3 showed a better performance towards ORR than pure Pt, its catalytic activity towards methanol oxidation reaction (MOR) is still low [186]. It is believed that the low MOR is due to the agglomeration/aggregation of the Pt/WO_3.

Addition of carbon materials to the Pt/WO_3 has been extensively investigated by most research groups to overcome the agglomeration issue of the Pt/WO_3 [186–190] and at the same time to maximize the utilisation thus enhance the electrocatalytic activity of the Pt/WO_3. This modification to Pt/WO_3 would not only improve the MOR activity but also enhance the ORR activity. The enhanced performance of Pt/WO_3/C towards ORR and MOR is believed to be attributed to the increase of specific surface area of the Pt/WO_3/C and the better dispersion of the nanoparticles after the addition of the carbon.

Tin oxide (SnO_2)

Tin oxide (SnO_2) is another non-carbon catalyst support with n-type semiconductor properties (with varied electrical

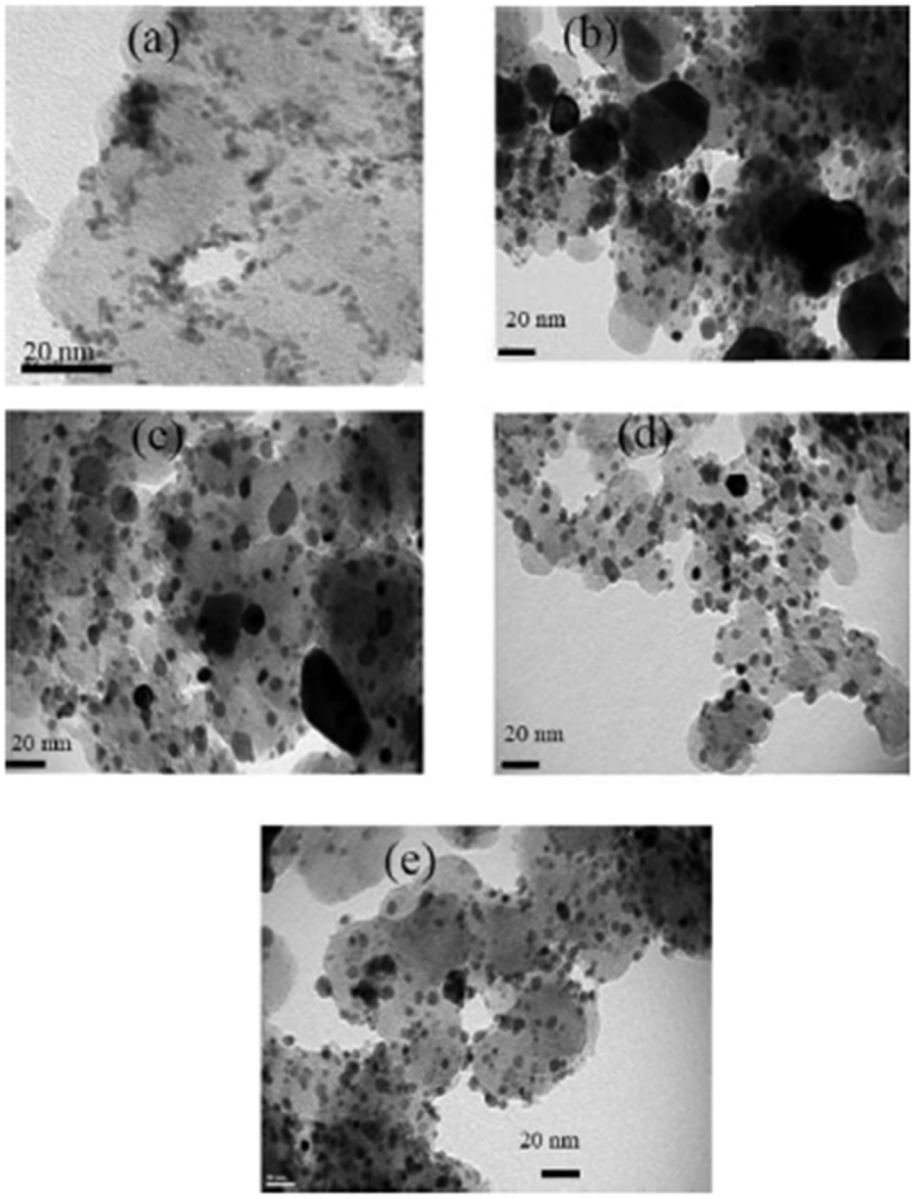

Fig. 7 – TEM images of Pt/TiO_2/C with varied Pt to Ti atomic ratios: (a) Pt/C, (b) Pt/C-750, (c) (3:1) Pt–TiO_2/C-750, (d) (2:1) Pt–TiO_2/C-750, and (e) (1:1) Pt–TiO_2/C-750. Reproduced with permission [173].

conductivity from 0.1 to 10^{-6} S cm^{-1}), a structure that is almost similar to TiO_2 which has also been used as support to Pt catalyst in fuel cell applications [183,191–193]. Various forms of SnO_2 were reported such as mesoporous SnO_2 by using neutral-surfactant template-assisted method, nanowire SnO_2 by using thermal evaporation method and nanocluster structure SnO_2 by using hard template method [193–195]. Pt nanoparticles were deposited on the mesoporous SnO_2, nanowire SnO_2 and nanocluster structure SnO_2 by using modified polyol method, electrochemical deposition and polyol method, respectively. The mesoporous SnO_2 studied by Zhang et al. (2010) [193] revealed the average size of SnO_2 nanoparticles to be ~6.1 nm and the average of Pt nanoparticles size to be ~5.2 nm. When Pt nanoparticles were deposited onto the SnO_2, BET analysis showed the decrease in specific surface area, pore size and pore volume because the Pt nanoparticles were incorporated within the pores of the SnO_2 thus blocking the pores passages. Not only Pt/SnO_2 showed a good performance towards ORR, it also showed enhance stability compared to Pt/C. Pt/SnO_2 lost only 50% ECSA after 5000 cycles while Pt/C lost almost 90% ECSA after 1000 cycles. Pt/SnO_2 has good dispersion of Pt nanoparticles and can create strong interaction between Pt metal and SnO_2 support which leads to an excellent ORR activity [193].

Unlike other oxides, SnO_2 can serve as an independent catalyst support without requiring a modification (e.g. addition of carbon material). We believe that it is due to the good interaction between SnO_2 and Pt metal (prevent agglomerations to occur, provide high surface area), high CO tolerance and other remarkable physicochemical properties of the SnO_2

support itself. Therefore, SnO_2 can be considered as an efficient and a robust catalyst support to Pt metal in various fuel cell applications.

Pt nanoparticle sizes and fuel cell performance of modified carbon-based and non-carbon-based support

The morphology of each electrocatalyst and the average size of Pt nanoparticles can be determined through SEM and TEM analysis, which are the two most commonly used methods to characterize the physical properties of electrocatalysts. Table 1 shows the average diameters of the Pt nanoparticles, ranged from that are dispersed on each modified carbon-based and non-carbon-based catalyst support from different synthesis routes.

The smallest Pt nanoparticle size was obtained when GNS was used as the support (Table 1). Despite the theoretical specific surface area of graphene of 1019 $m^2\ g^{-1}$, it has been reported elsewhere that its surface area is in fact much higher, i.e., 3400 $m^2\ g^{-1}$, making graphene a desirable carbon candidate for catalyst support [196,197]. Meanwhile, CNTs only exhibit specific surface areas between 50 and 1315 $m^2\ g^{-1}$, while graphite and diamond display specific surface areas between 7 and 380 $m^2\ g^{-1}$ and 8 and 52 $m^2\ g^{-1}$, respectively [198–200]. For non-carbon-based supports, SiC, TiO_2, IrO_2, WO_3 and SnO_2 exhibit relatively low specific surface areas, which range from 81 to 135 $m^2\ g^{-1}$, 150 $m^2\ g^{-1}$, 120–203 $m^2\ g^{-1}$, 50 $m^2\ g^{-1}$ and 23–194 $m^2\ g^{-1}$ respectively [201–206]. It should also be noted that a catalyst support should have a specific surface area equal to or greater than 100 $m^2\ g^{-1}$ for the good dispersion and utilisation of Pt nanoparticles to attain high performance in fuel cells [200].

The size of Pt nanoparticles and Pt conformation are two of the most important factors that could greatly influence the activity and durability of fuel cells [207,208]. The smaller the Pt particles size, the lower the durability towards load cycles [208–211], the higher the fraction of surface atoms interacting with the support (carbon atoms) compared to the larger particles thus improve the charge transfer and enhance the catalytic activity [212]. Matsutani et al. (2010) [213] reported that when the Pt nanoparticles size increased from 2–3 nm to 4–5 nm due to the heat treatment, an improved durability of Pt towards PEMFC load cycle was observed. However, based on a few reports, heat treatment could also broaden the particles size distributions, which could affect the fuel cell performances [207,210]. Other than that, increasing the size of Pt nanoparticles could also increase the vacancy availability of Pt sites for the adsorption of oxygen and cause the reactive intermediates to form [211]. Due to these issues, Li et al. (2014) [211] argued that, to exhibit high specific catalytic activity, a catalyst should exhibit not only low nanoparticles size and high surface area of support but also several other features: (i) Pt nanoparticles must be uniform in size; (ii) uniform dispersion of Pt nanoparticles on the support; and (iii) electrochemical condition used for "pre-conditioning" of nanoparticles for determining the ECSA and the catalytic activity must follow the same route.

As mentioned earlier, it is widely known that the particles size of Pt has a great influence on the fuel cell performance. However, there are a few factors that need to be considered in order to obtain the optimum Pt nanoparticles size such as Pt precursors, the methods applied and the reducing agents used. The most common Pt precursors used by researchers are hexachloroplatinic acid (H_2PtCl_6), tetraammineplatinum (II) chloride ($Cl_2H_{12}N_4Pt$) and ammonium hexachloroplatinate ($(NH_4)_2PtCl_6$. They are soluble in water and have low decomposition temperatures of 350 °C, 375 °C and 320 °C, respectively [214,215]. The ethylene glycol reduction method (also known as polyol method) is one of the most common, simple and straightforward methods used to synthesis Pt-based electrocatalyst [10,28,125,216,217]. Ethylene glycol is preferred because it acts not only as a reducing agent but also as a dispersing agent to the catalyst. It is also mild and environmental friendly [218]. Studies revealed that when ethylene glycol was used as the solvent and reducing agent, the nanoparticles obtained tend to be smaller in size and displayed better dispersion on the support [10,56–58,101,165,219]. Besides ethylene glycol reduction method, heat treatment is another method that is usually used by researchers to synthesis Pt-based electrocatalyst [103,137,220]. However, the heat treatment method normally gives rise to uneven dispersion and bigger size of Pt nanoparticles onto the support that causes the mass activity to decline with the operation time [221].

When Pt catalyst is supported with carbon-based supports (CNTs, graphite, graphene, etc.), their interaction is believed not only to modify the physicochemical properties and its electronic conductivities but also at the same time enhancing the catalytic activity and stability of the electrocatalyst. The modifications of the carbon support increase the specific surface area that will provide a good basis for the dispersion of the Pt nanoparticles. That is the main reason why carbon-based support gained an extensive interest. In oppose to the non-carbon supports (SiC, TiO_2, WO_3 and etc.), they have very low electronic conductivity that limits their contribution on the catalytic activity. Moreover, their specific surface area that are obviously lower than carbon-based supports is another reason why the usage of non-carbon supports is still hindered. The addition of carbon to the non-carbon supports in order to enhance the electrical conductivity in a few studies revealed that non-carbon supports still do not have the ability to be an independent support. However, non-carbon supports (especially metal oxides) displays good corrosion resistance and good thermal and mechanical stability, thus showing a high potential to be a good catalyst support for fuel cell applications [183]. Intensive studies on the modifications of non-carbon supports should be emphasized in order to make them an efficient catalyst support and have sufficient properties of fuel cell materials.

In fuel cells, especially PEMFCs and DMFCs, the ORR occurs at the cathode side. The ORR can be evaluated in either an alkaline or an acidic media depending on purposes and applications. The ORR can occur *via* two major pathways, i.e., a 2-electron pathway (preferable in industries such as microbial production, hydrogen peroxide production, textiles, etc.) [222–224] and a 4-electron pathway (preferable in fuel cell applications) [225]. 2-electron pathway is not preferred in fuel cells because the H_2O_2 is produced as the intermediate product. It is considered as a poisonous substance that will

Table 1 – Average size, fuel cell performance and durability of Pt nanoparticles supported on carbon-based and non-carbon-based supports.

Supported Catalyst	Synthesis routes	Metal loading/ wt%	Average Pt particle size (nm)[a]	Fuel cell performance and durability	Measurement conditions	Ref.
Pt/C Pt/CNT	Wet oxidation, reduction	20	2.8 2.7	(PEMFC): Accelerated durability test: Pt/CNT- ESA decreases 26.1%, Pt/C- ESA decreases 49.8%; degradation rate Pt/C larger (1.9 times) than Pt/CNT.	192 h, 0.5 M H_2SO_4, 20 ± 1 °C, scan rate 0.01 V s^{-1}, electrode area 2.3 × 2.3 cm^2	[25]
Pt/GSP Pt/CNT Pt/XC-72	Ethylene glycol reduction	20	2.3	(PEMFC): ESA values are 50.2, 49.9 and 52.2 m^2 g^{-1} for Pt/GSP. Pt/CNT and Pt/XC-72 respectively; ORR current only degrades 19% for Pt/GSP at 0.9 V compared to 40% and 57% for Pt/CNT and Pt/XC-72 respectively.	0.5 M H_2SO_4 (10 mV s^{-1}), N_2 atmosphere	[10]
Pt/MWCNT Pt/XC-72	Ethylene glycol reduction	10	2.0–5.0	(DMFC): Limited current density of 434 and 309 mA cm^{-2} for Pt/MWCNT and Pt/XC-72 respectively; maximum power density of 103 and 70 mW cm^{-2} for Pt/MWCNT and Pt/XC-72 respectively.	90 °C, methanol concentration of 1.0 M, flow rate of 1.0 mL min^{-1}, 0.2 MPa O_2	[28]
Pt/MWCNT	Ethylene glycol reduction	30	2.5	(PEMFC): Corrosion only 5.7% for Pt/MWCNT and 9.0% for Pt/XC-72 after 1000 h; loss of Pt surface (MWCNT) is 37% and (XC-72) is 80% after 168 h oxidation treatment.	60 °C, N_2 purged 0.5 M H_2SO_4, 0.9 V	[217]
Pt/NCNT	Ethylene glycol reduction	30	4.2	(PEMFC): Initial ESA Pt/NCNT, Pt/CNT and Pt/C retain 42.5%, 11.2% and 4.6%, respectively after 4000 cycles.	0.5 M H_2SO_4, scan rate 50 mV s^{-1}	[125]
Pt/NCNT	Ethylene glycol reduction	30	4.2	(PEMFC): Pt/NCNT showed current density of 0.230 A cm^{-2} higher than Pt/CNT (0.144 A cm^{-2}), Maximum power density of Pt/NCNT (0.876 W cm^{-2}) larger than Pt/CNT (0.470 W cm^{-2}).	0.5 M H_2SO_4, scan rate 5 mV s^{-1}	[216]
Pt/NCNT	In situ reduction	13	3.0–4.0	(PEMFC): For ADT test, after 1500 cycles, Pt/NCNT specific activity is 0.141 vs 0.150 mA cm^{-2} and its mass activity is 0.1085 vs 0.1110 mA μg^{-1}, which is 1.6 and 4 times larger than Pt/C, respectively.	0.1 M $HClO_4$, scan rate 10 mV s^{-1}	[127]
Pt/NCNT	Hydrothermal treatment	3.95 at%	6.0	The conversion of cinnamaldehyde using Pt/NCNT as catalyst (at 2.5 MPa of pressure and 300 min of total time of reaction) increased up to 6 times with respect to the value obtained with MWNTs-NCNT and MWCNTs. The conversion increased further with a pressure of 5 MPa for the same Pt/NCNT catalyst, reaching 80% in just over 200 min.	Hydrogen with pressures of 2.5 and 5 MPa and 100 °C with 100 mL of isopropanol as solvent, 2 g of cinnamaldehyde	[137]
Pt/NG	In situ one step method	14	2.5	(DMFC): The mass specific oxidation current for Pt/NG-300, Pt/G-300 and Pt/G-800 is 40 mA mg^{-1}, 41 mA mg^{-1} and 34 mA mg^{-1}, respectively.	1 M H_2SO_4 and 1 M CH_3OH, scan rate 20 mV s^{-1}	[140]
Pt/NG	Electroless deposition route	6.58 at%	2.0–6.5	(DMFC): The onset potential for methanol oxidation is about 0.4 V for Pt/NG and about 0.5 V for the Pt/G, indicating higher MOR activity for the Pt/NG catalyst. The anodic current peak occurs at around 0.67 V for both samples and the peak current for methanol electrooxidation increases with increasing scan rate. At a scan rate of 50 mV s^{-1}, the forward peak current for Pt/NG is about 4 times higher than that of the Pt/G.	1 M CH_3OH and 0.5 M H_2SO_4, with scan rates of 10, 20, 50,100 and 200 mV s^{-1}	[141]
Pt/NG	Ethylene glycol reduction	0.063 mg cm^{-2}	~8.0	(Biosensor): Pt/NG showed the increase in oxidation current of homocysteine at 0.63 V, 210 mV less positive potential shift and 3 times higher oxidation current compared to Pt/G.	N_2 atmosphere, at room temperature, scan rate 50 mV s^{-1}	[145]
Pt/BG	Sodium borohydride	35	8.0	(PEMFC): 2.2 times higher performance compared to Pt/G, maximum power density of 373 mW cm^{-2} at 70 °C without 15 psi back pressure.	0.1 M $HClO_4$, scan rate 50 mV s^{-1}	[149]
Pt/BG	Polyol	35	5.0	(PEMFC): 2.4 times higher performance compared to Pt/G, maximum power density of 412 mW cm^{-2} at 70 °C without 15 psi back pressure.	0.1 M $HClO_4$, scan rate 50 mV s^{-1}	[149]
Pt/BG	Modified polyol method	35	4.3	(PEMFC): 3.3 times higher performance compared to Pt/G, maximum power density of 565 mW cm^{-2} at 70 °C without 15 psi back pressure respectively. Delivers the current density of 320 mA cm^{-2} at 0.5 V for 50 h (durability test).	0.1 M $HClO_4$, scan rate 50 mV s^{-1}	[149]

Pt/BG	Microwave-assisted polyol	40	2.7	(DMFC): Onset potential and peak potential for CO oxidation negatively shifted about 60 mV and 23 mV, respectively (compared with Pt/G) Initial ESA for Pt/BG retains 76.5% and 61.0% for Pt/G.	0.5 M H_2SO_4, scan rate 50 mV s^{-1} [148]
Pt/SG	Modified ethylene glycol	20	ND	ND	0.1 M $HClO_4$ electrolyte at 30 °C, scan rate 50 mV s^{-1} [159]
Pt nanowire/SG	Solvothermal	50	2.0	(PEMFC): After 3000 cycles, PtNW/SG loses only 42% of its initial ECSA, whereas the losses in ECSA for PtNW/G and Pt/C are 72% and 99%, respectively. PtNW/SG showed a very high specific activity of 0.675 mA $cm^{-2}{}_{Pt}$ compared to PtNW/G and Pt/C that displayed the specific activity values of 0.543 and 0.250 mA $cm^{-2}{}_{Pt}$, respectively.	0.1 M $HClO_4$, scan rate 50 mV s^{-1} [220]
PtAu/MWCNT	Reverse micro-emulsion	20	2.0	(PEMFC): Max power density: PtAu/MWCNT is 625 mW cm^{-2} at 0.426 V, Pt/C is 355 mW cm^{-2} at 0.499 V.	0.5 M H_2SO_4, scan rate 100 mV s^{-2} [27]
PtRu/SWCNT	Single-pot	0.4 mg cm^{-2}	NA	(DMFC): Max methanol oxidation current is 50–60 mA cm^{-2}; power density of 45 mW cm^{-2} greater than PtRu (28 mW cm^{-2}).	70 °C, 1 M H_2SO_4, N_2 purged 30 min, scan rate 20 mV s^{-1} [31]
Pt-RuO_x/BDD	Sol-gel method	20	500.0 nm and 5.0 μm (SEM)	(DMFC): Methanol oxidation with onset potential 20 mV lower than commercial Pt-Ru/C.	0.5 M methanol in 0.5 M H_2SO_4 [45]
PtRu/BDD	Sequential electrodeposition	20	374.0–774.0 (SEM)	(DMFC): The characteristic current features for platinum, hydrogen adsorption and desorption (100 to −250 mV), Pt oxide formation (700 −1000 mV), and Pt oxide reduction (550 mV). The maximum current densities for methanol oxidation were in the range of 190–101 mA cm^{-2} and 176–78 mA cm^{-2}.	1 M CH_3OH in 0.5 M H_2SO_4, scan rate 500 mV s^{-1} [235]
Pt/B-UNCD	Wet chemical method	20	4.0–5.0	(PEMFC): The exchange current density is 1.14×10^{-10} A cm^{-2}, the mass activity of the conductive diamond powder supported Pt is 0.09 (A $mg^{-1}{}_{Pt}$) comparable to reported for carbon-supported Pt. B-UNCD powder exhibits less Pt surface area loss without sacrificing catalytic activity.	0.5 M H_2SO_4, scan rate 5 mV s^{-1} [236]
Pt/BDD	Electroless method	20	30.0–50.0 (SEM)	(PEMFC): Reduction peak at 0.4 V, fast decay of ECSA of only 7% is observed, followed by a quite stable ECSA after 200 potential cycles, exhibited high sensitivity towards H_2O_2 detection in the range of 1–400 μM with the detection limit of 9.0 μM.	0.5 M H_2SO_4, scan rate 50 mV s^{-1} [237]
Pt/GSP	Ethylene glycol reduction	20	2.2	(PEMFC): The values of ESA are 52.2, 49.5, and 50.2 m^2 g^{-1} for Pt/XC-72, Pt/CNT, and Pt/GSP, respectively. The ORR activity at 0.90 V is 17.3, 16.7, and 20.4 A g^{-1} for Pt/XC-72, Pt/CNT, and Pt/GSP, respectively. The ESA degraded by 58%, 47% and 32% for Pt/XC-72, Pt/CNT, and Pt/GSP, respectively.	0.5 M H_2SO_4, scan rate 50 mV s^{-1} [10]
Pt/GNF	Ethylene glycol	50	3.0	(PEMFC): Loss of Pt surface (GNF) is 40.2% and (XC-72) is 68.9% after 150 cycles oxidation treatment.	80 °C, 1.2 V [52]
Pt/NFGNF	Ethylene glycol reduction	20	2.0–5.0	(PEMFC): Pt/NFGNF showed the peak power density of 867 mW cm^{-2} at 70 °C and 2-bar pressure. For the Pt/C and Pt/GNF catalysts, the loss in ECSA after 10000 potential cycles is ~67%, whereas the losses in ECSA are about 29% and 12% for Pt/NGNF and Pt/NFGNF catalysts, respectively.	0.5 M $HClO_4$, 50 mV s^{-1} [57]
Pt/NSG	Ethylene glycol	350 μg cm^{-2}	2.3	(PEMFC): Mass activity loss is 45.3% (Pt/XC-72 loss 84.2%) after 1500 cycles.	0.1 M $HClO_4$, N_2 purged, room temperature, sweep rate 20 mV s^{-1} [58]

(continued on next page)

Table 1 – (*continued*)

Supported Catalyst	Synthesis routes	Metal loading/ wt%	Average Pt particle size (nm)[a]	Fuel cell performance and durability	Measurement conditions	Ref.
Pt/MGO	Pulse-microwave-assisted polyol route	ND	3.5	(PEMFC): CV results showed that the initial ECSA of Pt/MGO catalyst is 29.0 $m^2 g^{-1}$pt, higher than Pt/CB (11.7 $m^2 g^{-1}$pt). For durability test, after 1000 CV cycles, the ECSA loss of the Pt/MGO catalyst is 2.07%, much lower than those of the Pt/CB catalyst and Pt/GC catalyst (23.08% and 19.61%, respectively).	0.5 M H_2SO_4, scan rate 10 mV s^{-1}	[56]
Pt/GNS	Simultaneous reduction by ethylene glycol	20	1.2	(PEMFC): Displayed current density of 0.9 mA cm^{-2}.	0.1 M $HClO_4$, scan rate 10 mV s^{-1}	[238]
Pt/GNS	Chemical oxidation and subsequent thermal exfoliation	80	<3.0	Current density of methanol electrooxidation of Pt/GNS catalyst was at least twice as large as observed in Pt/C catalyst. Pt/GNS catalyst also maintained high Pt mass activities with increased Pt loading on the working electrode, ranging from 0.2 to 2.0 mg cm^{-2}.	0.5 M H_2SO_4, scan rate 50 mV s^{-1}	[93]
Pt/GNS	Pyrolysis	20	2.0–3.0	Methanol oxidation reaction: CO oxidation peak not observed after 30 s CO flow.	0.05 M H_2SO_4, room temperature, sweep rate 5 mV s^{-1}	[103]
Pt/rPGO	Colloidal method	20	3.0	(PEMFC): Pt/rPGO displays 15.5 times mass diffusion rate than that of the Pt/rGO causes the Pt/rPGO catalyst to exhibit 1.5 times higher in Pt mass activity toward ORR compared with the Pt/rGO. After H_2 thermal treatment, the mass activity of the Pt/rPGO increases to 1.9 times that of the Pt/rGO. Pt/rPGO catalyst provides higher ECSA (74.4 $m^2 g^{-1}$) than that of the Pt/rGO and Pt/C catalysts (64.7 $m^2 g^{-1}$ and 61.2 $m^2 g^{-1}$, respectively), after 3000 cycles, ECSA of Pt/rPGO remains 40.7% (higher than Pt/rGO, 25.6%).	0.5 M H_2SO_4, scan rate 50 mV s^{-1}	[9]
Pt/G	Reduction in one pot	45	5.0–6.0	(DMFC): ECSA for the Pt/G was higher than Pt/Vulcan (44.6 and 30.1 $m^2 g^{-1}$ Pt, respectively), the peak current density of Pt/G at the potential of 0.652 V was 199.6 mA mg^{-1} Pt. During the forward potential scanning. process on Pt/G, which is nearly twice of that on Pt/Vulcan (101.2 mA mg^{-1} Pt at 0.664 V), while its current-peak potential is about 12 mV lower than that of Pt/Vulcan.	0.5 M H_2SO_4, scan rate 50 mV s^{-1}	[99]
Pt/G	Reduction by $NaBH_4$	10	5.0	(DMFC): Limiting current of 0.2 V; ending current of 55.5 mA mg^{-1} after 1200 s.	0.5 M H_2SO_4, room temperature, scan rate 20 mV s^{-1}	[239]
Pt/G/CB	Ethylene glycol reduction	20	2.0–6.0	(PEMFC): The mass activity was 3.9 times higher and 65% improvement of the performance measured at $E_{cell} = 0.4$ V was achieved when CB was added.	The cathode was cycled at 50 mV s^{-1} between 0.02 and 1.1 V vs. SHE	[101]
Pt/FGS	Impregnation method	20	2.0	(PEMFC): ESA decrease (62.4% of initial ESA value) after 5000 cycles degradation.	0.5 M H_2SO_4, scan rate 50 mV s^{-1}	[240]
Pt/SiC Pt/SiC/C	Ethylene glycol reduction	20	~3.0 3.0–8.0	(PEMFC): Pt/SiC-no visible H adsorption and desorption peak after 1000 cycles; ESA value of 13 $m^2 g^{-1}$. Degradation of Pt/SiC/C was 42.7% after 1000 cycles; ESA value of 48 m^2/g; 22.5% of initial ESA remains after 4000 cycles.	0.5 M H_2SO_4, scan rate 50 mV s^{-1}	[165]
Pt/SiC-NS Pt/SiC-SPR	Polyol method	20–22	4.0–5.0 5.0–8.0	(PEMFC): ESA values of Pt/SiC-NS and Pt/SiC-SPR are 55.8 and 35.6 $m^2 g^{-1}$, respectively.	0.5 M $HClO_4$, scan rate 50 mV s^{-1}	[11]
Pt/TiO_2	Colloidal method	0.4 mg cm^{-2}	6.2	(PEMFC): Max power density is 0.94 W cm^{-2}; no corrosion and potential loss after 200 h; ESA loss is 20% after 80 h.	75 °C, flow rate H_2 and O_2 150 mL min^{-1}, 1.2 V	[171]

$Pt/TiO_2/C$	Phase transfer synthesis	10	1.8–3.0	(PEMFC): $Pt/TiO_2/C$ composite, with a total loading of 10 wt% Pt and 50 vol% C, was highly stable during the thermal treatment of 1000 h in 170 °C followed by 4000 h in 210 °C. Enhanced double layer capacitance in the electrode. Increased ORR current density when carbon content is increased because of the sufficient high macroscopic electronic conductivity in $Pt/TiO_2/C$.	Polarization curves were recorded with 100% H_2 flowing over the CE (10 mV s^{-1}) but in the cyclic voltammetry measurements the CE was fed with 5% H_2 in Ar (100 mV s^{-1})	[167]
$Pt/TiO_2/Ru$	Borohydride reduction	20	3.0	(PEMFC): ESA 30 m^2 g^{-1}; onset potential and half wave potential shift to positive potentials by ~45 mV; mass activity of 167 mA mg^{-1} at 0.9 V; specific activity of 558 μA cm^{-2} at 0.9 V.	25 °C, N_2 purged, 0.5 M $HClO_4$, sweep rate 20–100 mV s^{-1}, rotation rate 1600 rpm	[172]
$Pt/TiO_2/W$	Suspend the oxide in methanol solution of H_2PtCl_6, reduction in excess $NaBH_4$ (under N_2 purge)	25	NA	(PEMFC): The RDE curve of $Pt/TiO_2/W$ is identical to Pt/C and also showed activity that was very similar to the Pt/C.	0.1 M H_2SO_4	[4]
Pt/IrO_2	Chemical reduction	5	5.0	(URFC): The fuel cell power density is 1160 mW cm^{-2} at 2600 $mAcm^{-2}$. The overall performance is close to that with the commercial Pt/C and about 1.8 times higher than that with the conventional Pt/IrO2 catalyst. The cell performance for water electrolysis is also slightly improved, which is due to the lower interparticle catalyst resistance with 5 wt% Pt on IrO_2 compared to no Pt on IrO_2.	80 °C with H_2/O_2 at pressure of 0.2 MPa	[180]
Pt/IrO_2	Ultrasonic polyol method	22.75	3.0–6.5	(URFC): Maximum current density of 540 mA cm^{-2} at terminal cell voltage of 1.8 V and shows a limiting current density of 342 mA cm^{-2}.	At room temperature, feeding dry H_2 and air at a flow rate of 50–150 scc min^{-1}	[178]
$Pt/Ir\text{-}IrO_2$	Microwave-assisted polyol	50 mol% Pt and 50 mol% Ir	2.6–2.8	(URFC): $Pt/Ir\text{-}IrO_2$ catalyst possesses the highest ECSA (24.74 m^2 g^{-1}) and the highest activity towards ORR (21.71 mA mg^{-1} at 0.85 V) and also high activity towards OER (42.35 mA mg^{-1} at 1.55 V). Kinetic analyses indicate that ORR on $Pt/Ir\text{-}IrO_2$ catalyst follows four-electron mechanism.	0.5 M H_2SO_4, scan rate 5 mV s^{-1}	[181]
Pt-Ir/TiC	Modified ethylene glycol colloidal	26.7	5.3	(PEMFC): Chronopotentiometry studies revealed no short term degradation of the TiC support. LSV results of Pt-Ir/TiC showed the highest kinetic current per mass of metal (164 mA mg^{-1}_{metal}) at 0.9 V during ORR. However, for OER activity at 1.55 V, the supported Ir/TiC had one to two order of magnitude higher kinetic current per mass of metal than unsupported Ir black and Pt-based electrocatalysts, respectively. Pt-Ir/TiC also showed 65% round-trip, a far superior electrocatalyst activity compared to the bifunctional electrocatalysts for URFC systems literature.	0.1 M $HClO_4$, scan rate 50 mV s^{-1}	[241]
Pt/WO_3	Microwave-assisted ethylene glycol	20	7.0	(DMFC): Peak potential of methanol oxidation on Pt/WO_3 is 50 mV more negative than that of commercial Pt/C. The difference between the potentials for the forward and backward sweeps is smaller on Pt/WO_3 (160 mV) than on commercial Pt/C (258 mV). Pt/WO_3 also showed a higher mass activity (684 A g^{-1} Pt) which is 2.3 times of that of commercial Pt/C catalyst.	0.5 M H_2SO_4–0.5 M CH_3OH solution, scan rate 20 mV s^{-1}	[242]
Pt/WO_3	Modified ethylene glycol colloidal	10 μg cm^{-2}	1.9	(DMFC): The oxidation of methanol started near 0.378 V and reached a peak at about 0.656 V. The Pt:W ratio of 1: 1 showed the highest peak current density of 1.2 A mg^{-1} Pt.	0.5 M H_2SO_4, scan rate 50 mV s^{-1}	[219]

(*continued on next page*)

Table 1 – (*continued*)

Supported Catalyst	Synthesis routes	Metal loading/ wt%	Average Pt particle size (nm)[a]	Fuel cell performance and durability	Measurement conditions	Ref.
Pt/WO_3	Reduction with methanal	40	13.2 (crystallite size from XRD analysis)	(PEMFC): The activity of IrO_2 was stable over the 100 oxidation cycles.	0.5 M H_2SO_4, 30 °C	[185]
$PtPd/WO_3$-CNF	Borohydride reduction	20	7.8	(PEMFC): $PtPd/WO_3$-CNF showed higher current than that of $PtPd/WO_3$ coated carbon black. $PtPd/WO_3$-CNF also displayed highest Ohmic resistance values of 0.363 and 0.713 Ω cm^{-2} at the voltage 0.2 and 0.4 V, respectively.	0.2 M H_2SO_4 electrolyte	[188]
Pt/WO_3-C	Chemical method	1.76 mg cm^{-2}	2.0–3.0	(PEMFC): Maximum power density obtained was 221 mW mg^{-1}. ESA value of 82 m^2 g^{-1} higher than Pt/C (74 m^2 g^{-1}).	0.5 M H_2SO_4, scan rate 50 mV s^{-1}	[187]
Pt/WO_3-C	Co-impregnation reduction	20	4.6	(DEFC): Pt/WO_3-C catalyst prepared by co-impregnation/ethylene glycol method showed the significant anodic peak current density at peak potential of 1.0 V vs. NHE during the positive potential sweep of CV curve (32.6 mA cm^{-2}), 1.4 and 2.9 times as high as those of the other two catalysts prepared by co-impregnation/$NaBH_4$ and co-impregnation/HCOOH reduction methods, respectively.	1 M CH_3CH_2OH and 0.5 M H_2SO_4, separately. Scan rate of 0.05 V s^{-1}	[189]
Pt/WO_3-C	Colloid-reduction	12–19	~5.0	(DMFC): The oxidation peak of ethanol for Pt/WO_3-C is higher than Pt/C. During the backward sweep process, an anodic peak is detected at 0.56 V for Pt/WO_3-C which is higher than Pt/C (0.52 V).	0.5 M H_2SO_4–0.5 M C_2H_5OH solution, scan rate 50 mV s^{-1}	[190]
Pt/WO_3-CNT	Thermal treatment	16.5 μg cm^{-2}	5.0	(DMFC): The onset of methanol oxidation starts around +0.1 V and peaks at +0.7 V with a peak current density of 98.5 mA cm^{-2} which is higher than Pt/CNT without WO_3 (14 mA cm^{-2}).	1 M H_2SO_4–1M CH_3OH solution, scan rate 50 mV s^{-1}	[186]
Pt/SnO_2	Polyol method	14	1.0–3.0	(PEMFC): The Pt/SnO_2 catalyst reserved 89.7% of its initial ECSA under 10 h potential hold at 1.6 V. The polarization curves indicated a comparable cell performance with Pt/SnO_2 anode and the commonly used Pt/C anode. Even at high current of 1 A cm^{-2}, the voltage of the single cell with Pt/SnO_2 anode remains very close to that with Pt/C.	0.5 M H_2SO_4, scan rate 50 mV s^{-1}	[195]
Pt/SnO_2	Colloidal method	20	3.0	(PEMFC): ECSA of Pt/SnO_2 remained above 10 m^2 g^{-1} even after 10,000 cycles The kinetic current density remained more than one-half of the initial values after 4000 cycles	0.1 M $HClO_4$, scan rate 50 mV s^{-1}	[243]
Pt/SnO_2	Impregnation method	60	6.3	(PEMFC): Both the anodic current due to the adsorption of oxygen and the formation of the platinum oxides (>ca .0.8 V) and the cathodic current due to the reduction of platinum oxides and the desorption of oxygen (>0.7 V) gradually decreased.	1.0 M H_2SO_4, scan rate 50 mV s^{-1}	[191]
Pt/SnO_2	Impregnation method	20	3.4	(PEMFC): Pt/SnO_2 and Pt/C catalysts were degraded with the presence of CO in hydrogen. However, the degradation of Pt/SnO_2 with 100 ppm CO was insignificant as compared with that of Pt/C.	Cell temperature of 75 °C	[192]
Pt/SnO_2	Electrochemical deposition	0.12 mg cm^{-2}	4.0–6.0	(PEMFC and DMFC): The ORR peak current of Pt/SnO_2 is about 13.3 mA mg^{-1} Pt which is 1.6 times larger than that of Pt/C electrode. The specific activity of Pt/SnO_2 is 0.025 mA cm^{-2} Pt that is slightly higher than the conventional Pt/C electrode (0.023 mA/cm^{-2} Pt). For MOR activity, two oxidation peaks related to the oxidation of methanol and intermediates appeared at ca. 0.68 and 0.51 V, respectively. The MOR peak current for the Pt/SnO_2 carbon paper electrode is about 71.5 mA mg^{-1} Pt, which is higher than that of the Pt/C electrode (65.0 mA mg^{-1} Pt).	0.1 M H_2SO_4, scan rate 50 mV s^{-1}	[194]

Pt/SnO_2	Modified polyol method	0.5 mg cm^{-2}	5.2	(PEMFC): The current density of Pt/SnO_2 at 0.7 V reached to 0.61 A cm^{-2} with maximum power density of 0.74 W cm^{-2}. The fuel cell performance of the Pt/SnO_2 was comparable to that of the Pt/C catalyst (current density and maximum power density of 0.72 A cm^{-2} and 0.81 W cm^{-2}, respectively). Pt/SnO_2 catalyst lost almost 50% if initial ECSA after 5000 cycles, whereas Pt/C lost nearly 90% of the initial ECSA after only 1000 cycles.	0.5 M H_2SO_4, scan rate 50 mV s^{-1}	[193]

[a] Based on TEM analysis, MGO- microcrystalline graphite oxide, GNS- graphene nanosheets, rPGO- reduced pore graphene oxide, CB-carbon black, NS- reaction of carbon with silicon monoxide, SPR-solid phase reaction, B-UNCD-boron-doped ultrananocrystalline diamond, NSG – nanoscale graphite, FGS- functionalized graphene sheet, ESA-electrochemical surface area, DEFC- direct ethanol fuel cell.

jeopardize the catalytic activity. In alkaline electrolyte, the mechanisms of 2-electron and 4-elecron pathways are shown as below [225]:

$$O_2 + H_2O + 4e^- \rightarrow 4OH^{-1}$$

$$O_2 + H_2O + 2e^- \rightarrow HO_2^- + OH^-$$

$$HO_2^- + H_2O + 2e^- \rightarrow 3OH^-$$

In acidic electrolyte, the mechanisms of 2-electron and 4-elecron pathways are as shown as below [225]:

$$O_2 + 4H^+ + 4e^- \rightarrow H_2O$$

$$O_2 + 2H^+ + 2e^- \rightarrow H_2O_2$$

$$H_2O_2 + 2H^+ + 2e^- \rightarrow 2H_2O$$

The ORR activity is recommended to occur at potentials as close as possible to the reversible electrode potential with sufficient reaction rate [225]. Mayrhofer et al. (2005 & 2008) [226,227] revealed that the dependence of the potential of zero total charge (pztc) is one of the ways to explain the effect of particles size on the ORR performance. They compared the ORR activity on the Pt nanoparticles and on the Pt supported carbon (surface). When the particles size decreases, the pztc shifted negatively from 0.285 V for Pt particles and 0.282 V for Pt with carbon support to about 0.245 V with a mean diameter of 1.25 nm. This shows that the anions adsorption energy (OH^-), was increased. In other words, decreased in particles size results the surface coverage by oxygenated species at the same potential increased. They also stated that the smaller particles with high oxophilicity tend to cause the decrease in surface area, due to the active sites blockage that is required for the adsorption of O_2 or the splitting of the O–O bond. Based on a few earliest studies on the Pt particles size, it can be concluded that the optimum particles size for excellent ORR activity was in the range 2–4 nm [228–231].

Usually, the ORR kinetics in fuel cells without catalyst presence are very slow. To achieve significant ORR performance, an active cathode catalyst is required [225]. Pt-based electrocatalysts are the current catalyst benchmark for ORR. To improve further, some modifications on the Pt catalyst have been performed such as alloying with other base metals (Ni, Co) or introducing carbon supports (CNT, CNF, graphene) [232–234]. Table 2 shows the fuel cell performances of Pt and their durability tests on modified carbon-based and non-carbon-based supports for fuel cell applications.

The high cost of Pt and the advantages of Pt-alloy catalyst

The selling prices of Pt

Large-scale commercialisation of fuel cells relies upon the fulfilment of three criteria, i.e., affordable cost, high performance and high durability [244]. Fig. 8 shows the worldwide Pt prices chart. Almost all research and development of fuel cells focuses on the performance enhancements of cathode catalysts and electrodes since generally the cathodic ORR is six orders of magnitude slower than the anode hydrogen

Table 2 – List of the prices for Pt-based and non Pt-based catalyst (based on year 2017 price).

Catalyst	Brand and product number	Weight (g)	Price (US$)	Surface area ($m^2 g^{-1}$)	Reference
Pt	BASF 590078–2	10	1470.00	25–34	[247]
80% Pt on C	PK catalyst 591778–2	10	1671.00	70 (total)	[248]
Pt black	HiSPEC 12755	5	1102.00	25–29.8	[249]
Pt black	Aldrich 570280	5	1327.00	25–34	[250]
Pt black	P1148-5 GM	5	1936.00	24	[251]
50% Pt on C	PK Catalyst 591578–2	10	1339.00	110 (total)	[252]
10% Pt on C	PK Catalyst 591078–2	10	481.00	220 (total)	[253]
10% Pt on C	HiSPEC 43876	10	694.00	105	[254]
10% Pt on C	Aldrich 738581	1	110.00	–	[255]
PtPd black	PK catalyst 3151626	5	1549.00	–	[256]
50% PtRu black	HiSPEC 41171	5	814.00	–	[257]
20% PtPd on C	PK catalyst 3151622	5	1179.00	–	[258]
40% Pt 20% Ru on C	HiSPEC 44172	10	1324.00	–	[259]
20% PtNi on C	PK catalyst 3152649	5	1089.00	–	[260]
20% PtRu on C	PK catalyst 592278–1	5	365.00	2–3	[261]
20% PtCu on C	PK catalyst 3151656	5	1089.00	–	[262]
20% PtSn on C	PK catalyst 3151670	5	1089.00	–	[263]
20% PtIr on C	PK catalyst 3151628	5	1299.00	–	[264]
20% PtCo on C	PK catalyst 3151646	5	1089.00	–	[265]
Pd black	PK catalyst 3151620	5	524.00	40–48	[266]
Pd black	P1002-5 GM	5	1230.90	–	[267]
Pd black	00659	5	441.00	20	[268]
Ru black	PK catalyst 3151606	5	719.00	34–38	[269]
20% Pd on C	PK catalyst 3151612	5	396.00	–	[270]
20% Ru on C	PK catalyst 3151602	5	399.00	180	[271]
5% Ru on C	R1622-5 GM	5	152.50	–	[272]
20% Au on C	PK catalyst 3151669	5	369.00	–	[273]
20% Fe on C	PK catalyst 3151684	5	590.00	–	[274]

oxidation reaction (HOR), thus requiring the cathode catalyst to contain eight-fold amount of Pt of the anode [245]. Cathode component is clearly the limiting component of the fuel cell [244]. Pt-based nanoparticles supported carbon is the current benchmark catalyst in both anode and cathode components. Table 2 shows the price comparison of Pt-based catalyst and non Pt-based catalyst.

The high cost of Pt has been the major limitation for years, and how to reduce the cost by reducing the cathode loading without compromising the durability and performance is always the main research subject in the field. Fuel cell vehicles cost millions to build and a typical electric car requires about 70–105 g Pt. For only 10 g of Pt it costs around 1000–2000 US$

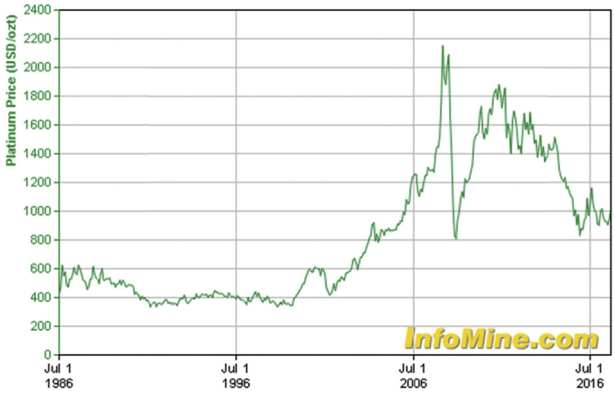

Fig. 8 – The worldwide price of platinum. Reproduced with permission [246].

which explain why large-scale application of fuel cell is still not realised. Besides the high cost, the other major problem is the activation loss on the oxygen side (cathode) [275]. Numerous studies have been performed to develop catalyst with high ORR catalytic activity. One of the most popular approaches is alloying Pt with other metals and suitable support.

Alloying Pt-based catalyst with other metals and nitrogen supported carbon and non-carbon materials for the enhancement of fuel cell performance

To address the aforementioned issue, two approaches can be performed without compromising the fuel cell performance, i.e., (i) reducing the Pt by alloying with transition metals such as cobalt, copper, nickel, gold, iron, ruthenium, etc. [276–283]; and (ii) adding heteroatom (nitrogen) to the Pt-alloy catalyst [284–286]. Reducing the Pt catalyst loading in some structures may lower the fuel cell performance, but the presence of a modified carbon support doped with highly active heteroatoms (N, S, B or P) could create stronger metal-support interactions and thus could maintain or increase the durability and catalytic activity of the fuel cells even under reduced Pt loading [120,287].

The improvement in the catalytic activity after introducing the transition metals to the Pt catalyst is contributed by a few aspects, i.e., (i) the shift in Pt-Pt interatomic distance; (ii) the change in the number of Pt closest neighbours; (iii) the adjustment in the vacancy of Pt 5d band; and (iv) the change in Pt metal content on particle surface [288]. Antolini (2007) has reviewed the capability of ternary catalysts formed by various selected transition metals to further enhance the catalytic activity of

Table 3 – Pt-alloy transition metals electrocatalyst and their structural characteristics.

Catalyst/Support	Synthesis route	Structural characteristics	Reference
PtM/C (M = Ni, Co and Cu)	Modified impregnation method	Nanoparticles of PtNi/C, Pt/Co/C, and PtCu/C were well dispersed. The particle size was 4.3, 5.8, and 6.3 nm for PtNi/C, Pt/Co/C, and PtCu/C, respectively.	[283]
PtM/C (M = Fe, Co, Ni and Cu)	Low temperature reduction	The particle size was 3.7, 3.6, 3.7, and 4.3 for PtFe/C, PtCo/C, PtNi/C, and PtCu/C, respectively.	[279]
PtAu/C	Co-reduction method	Presence of bimetallic PtAu. The particle size was 2.8 nm.	[277]
PtFe/C	Modified polyol method	Formation of Pt-Fe alloy catalyst. The average particle size was 3.6 nm	[278]
Pt/C/N-doped carbon (Pt/C/NC)	Thermal annealing	Pt/C/NC structure had uniformity. Formation of Pt/C covered with NC layers. The crystallite size of Pt nanoparticles depends on the annealing temperatures: 3.3, 5.7, 6.6, 7.7, and 9.4 nm for Pt/C/NC400, Pt/C/NC500, Pt/C/NC600, and Pt/C/NC700 °C, respectively.	[295]
PtFe/NMGC	Pyrolysis	Stable quaternary N type was dominantly observed in the NMGC incorporated with Fe. Pt nanoparticles in the range of 2–3 nm were well distributed on Fe-NMGC.	[286]
PtCo/NCNT	Pyrolysis	Nitrogen doped CNTs were twisted, entangled and well-integrated thus provide a conducting network as a catalyst support. Presence of Pt nanoparticles size in the range 7–10 nm, majority the nanoparticles consist of Pt but Co particles were also observed on the NCNTs support.	[284]
PtFeCo/C	Pyrolysis	Chemically ordered intermetallics of PtFeCo were observed. The particle size is the range of 3–4 nm for PtFeCo/C.	[280]
PtC/Pt-TiO_2	Reduction	Uniform dispersion of Pt particles on TiO_2 support. Particles size was measured to be 2.1 nm.	[296]
PtRu/graphene	Modified polyol method	Bimetallic PtRu particles were well dispersed on the graphene sheets with the average size less than 10 nm.	[297]
PtFe/graphene	Solution-phase self-assembly method	PtFe nanoparticles with an average size 7 nm were assembled on the graphene sheets.	[298]
PtAu/TiO_2/C	Post heat treatment	Bimetallic PtAu formed a very stable structure when heat was applied. The average particles size is 3.4 nm.	[299]
PtNb/TiO_2	Hydrothermal synthesis and borohydride reduction	Uniform distribution of the PtNb/TiO_2 was observed with an average particles size of 3 nm. Nb/TiO_2 showed dominant rutile crystal structure of TiO_2.	[300]

NMGC-nitrogen doped mesoporous graphitized carbon.

ORR Pt [288]. They reported that Pt-alloy catalyst either in bimetallic or tri-metallic form, could possess high ORR catalytic activity and at the same time lower the catalyst cost. Besides, the addition of N to the catalyst could alter the local electron density inside the electrocatalyst and initiate the N sufficient related active sites for the reaction to occur efficiently [40]. Alloying Pt with transition metals supported carbon or non-carbon based support is definitely an efficient way to enable the commercialisation of large-scale fuel cell technology. Table 3 shows the Pt-based electrocatalyst alloyed with transition metals supported carbon and non-carbon based support, together with the synthesis route and structural characteristics.

Most of the modified carbon-based catalyst supports have been studied given their (low cost, high specific surface area, long-term stability, attractive mechanical and electrical properties, and high catalytic activity in the ORR) [33,289]. Even so, most of the systems with Pt on modified carbon-based supports have exhibited outstanding performance only in alkaline media and not in acidic media, which continues to inhibit their full application in fuel cells. To overcome the existing gap, some advanced approaches have been devised, such as doping two heteroatoms such as sulphur and nitrogen to the modified carbon-based support and developing bimetallic/bifunctional or even tri-metallic (ternary) electrocatalysts [110,290–294]. Dual doping of heteroatoms into a modified carbon-based support could increase the synergetic effect and improve its catalytic activity in acidic media [110]. The development of an active electrocatalyst that can exhibit excellent performance in both alkaline and acidic media is extremely desirable to facilitate large-scale fuel cell commercialisation.

Conclusion and future perspectives

Numerous studies of potential catalyst supports have been performed, mainly focusing on carbon materials, with limited studies on non-carbon materials. This is due to the mechanical and chemical properties of the carbon material supports being more robust in acidic and alkaline conditions. The effects of the carbon support and the interactions of the carbon support, with Pt and Pt-alloy especially, are important to improve the catalytic activity and enhance the long-term durability of the electrocatalysts. The wide usage of carbon materials as catalyst supports in fuel cells is also supported by their high resistance to corrosion. This might be related to the degree of the graphitic nature within the structure itself, i.e., higher graphitic structure translates to higher corrosion resistance. Fewer studies have explored non-carbon catalyst supports in fuel cell applications given their low surface area, low electrical conductivity, and low thermal stability. Additional work in exploring new, potential catalyst supports is suggested for future studies to produce eco-friendlier catalysts with high resistance for high concentration conditions and to achieve excellent electrochemical activity of fuel cells, and energy-storage devices.

In this review, graphene appears to be the best state-of-of-the-art catalyst support. Its high specific surface area, which contributes to the excellent dispersion of catalyst nanoparticles, has attracted many researchers to explore the potential of graphene as one of the most active carbon supports in fuel cells. However, graphene easily lumped into multilayer sheets that can cause lowering in the surface area, thereby decreasing the electro-catalytic activity of the fuel cell. The multilayer properties of graphene will also affect the dispersion of the catalyst nanoparticles on the support. To obtain one-layer or few-layer graphene sheets, the stirring period can be extended. Other recent reports reveal the development of various routes to synthesise modified carbon-based supports and how their strong interactions with metal catalysts can enhance the performance of fuel cells. Future works to determine a suitable route for an effective electrocatalyst with a modified catalyst support should consider three aspects:

1) Low cost. A low material and synthesis can significantly reduce the total cost of the fuel cell and help to accelerate the fuel cell commercialisation.
2) Efficient synthesis procedure that can lead to an active electrocatalyst with high specific surface area and effective modified catalyst support (either carbon based or non-carbon based). The optimum parameters such as metal weight ratio, temperature, or precursors should be highlighted.
3) Molecular modelling. Modelling can provide insights into the interaction between the metal catalyst and its support, which includes the morphology, active binding sites, the dispersion of metal nanoparticles, and the electronic structure and conduction.

Although numerous effective electrocatalysts have been studied, there were only a few that exhibited good performance in acidic media. To overcome this limitation, recent studies have focused more on discovering other modifications of carbon material supports to grant enhanced capability and stability in acid conditions, better thermal stability, strong interactions with the catalyst that can enhance the electrocatalytic activity and extended fuel cell lifetimes. Moreover, studies of bimetallic electrocatalysts with suitable modifications and functionalisations of catalyst supports should be emphasized, as they are expected to exhibit excellent electrocatalytic activity in fuel cells because bimetallic electrocatalysts are more stable and can better prevent demetallation in acidic media relative to the single metal electrocatalysts.

In this report, we have reviewed the progress in the development of carbon and non-carbon support materials in fuel cell applications and how modifications enhance their physical and chemical properties. The prices of Pt-based materials in the market and how to overcome the drawbacks existed for fuel cell commercialisation have also been reviewed. Briefly, alloying the Pt and reduce the Pt loading can reduce the fuel cell cost while the suitable supporting materials can enhance the long-term durability and thus can achieve excellent catalytic performance.

Acknowledgements

This work is financially supported by the Universiti Kebangsaan Malaysia (UKM) through the University Research Grant (DIP-2017-024) and Human Capital Fund (MI-2018-02). This

work also cofinanced from the Ministry of Education Malaysia through the Long-term Research Grant Scheme (LRGS/2013/UKM-UKM/TP/01).

REFERENCES

[1] Kroto HW, Heath JR, O'Brien SC, Curl RF, Smalley RE. C60: Buckminsterfullerene. Nature 1985;318:162–3.
[2] Lázaro MJ, Calvillo L, Celorrio V, Pardo JI, Perathoner S, Moliner R. Study and application of carbon black Vulcan XC-72R in polymeric electrolyte fuel cells. Carbon black: production, properties and uses, vol. 41; 2011.
[3] Antolini E. Carbon supports for low-temperature fuel cell catalysts. Appl Catal B Environ 2009;88:1–24.
[4] Subban C, Zhou Q, Leonard B, Ranjan C, Edvenson HM, DiSalvo FJ, et al. Catalyst supports for polymer electrolyte fuel cells. Phil Trans R Soc A Math Phys Eng Sci 2010;368:3243–53.
[5] Vladimir S, Bagotsky A. Fuel cell problems and solutions. John Wiley and Sons, Inc. Publication; 2009.
[6] Copper CL, Koubek E. An experiment to demonstrate how a catalyst affects the rate of a reaction. J Chem Educ 1999;76:1714.
[7] Shao Y, Liu J, Wang Y, Lin Y. Novel catalyst support materials for PEM fuel cells: current status and future prospects. J Mater Chem 2009;19:46–59.
[8] Guha A, Lu W, Zawodzinski TA, Schiraldi DA. Surface-modified carbons as platinum catalyst support for PEM fuel cells. Carbon 2007;45:1506–17.
[9] Cheng K, He D, Peng T, Lv H, Pan M, Mu S. Porous graphene supported Pt catalysts for proton exchange membrane fuel cells. Electrochim Acta 2014;132:356–63.
[10] Zhang S, Shao Y, Li X, Nie Z, Wang Y, Liu J, et al. Low-cost and durable catalyst support for fuel cells: graphite submicron particles. J Power Sources 2010;195:457–60.
[11] Dhiman R, Johnson E, Skou EM, Morgen P, Andersen SM. SiC nanocrystals as Pt catalyst supports for fuel cell applications. J Mater Chem A 2013;1:6030–6.
[12] Wang YJ, Wilkinson DP, Zhang J. Noncarbon support materials for polymer electrolyte membrane fuel cell electrocatalysts. Chem rev 2011;111:7625–51.
[13] Shao Y, Yin G, Gao Y. Understanding and approaches for the durability issues of Pt-based catalysts for PEM fuel cell. J Power Sources 2007;171:558–66.
[14] Yu X, Ye S. Recent advances in activity and durability enhancement of Pt/C catalytic cathode in PEMFC: Part I. Physico-chemical and electronic interaction between Pt and carbon support, and activity enhancement of Pt/C catalyst. J Power Sources 2007;172:133–44.
[15] Wang YJ, Fang B, Li H, Bi XT, Wang H. Progress in modified carbon support materials for Pt and Pt-alloy cathode catalysts in polymer electrolyte membrane fuel cells. Prog Mater Sci 2016;82:445–98.
[16] Soo LT, Loh KS, Mohamad AB, Daud WRW, Wong WY. An overview of the electrochemical performance of modified graphene used as an electrocatalyst and as a catalyst support in fuel cells. Appl Catal A General 2015;497:198–210.
[17] Subramanian NP, Kumaraguru SP, Colon-Mercano H, Kim H, Popov BN, Black T, et al. Studies on Co-based catalysts supported on modified carbon substrates for PEMFC cathodes. J Power Sources 2006;157:56–63.
[18] Poh CK, Lim SH, Pan H, Lin J, Lee JY. Citric acid functionalized carbon materials for fuel cell applications. J Power Sources 2008;176:70–5.
[19] Trogadas P, Fuller TF, Strasser P. Carbon as catalyst and support for electrochemical energy conversion. Carbon 2014;75:5–42.
[20] Iijima S. Helical microtubules of graphitic carbon. Nature 1991;354:56–8.
[21] Ebbesen TW. Carbon nanotubes: preparation and properties. CRC press; 1996.
[22] Koziol K, Boskovic BO, Yahya N. Synthesis of carbon nanostructures by CVD method, in carbon and oxide nanostructures. Springer; 2010. p. 23–49.
[23] Satishkumar B, Govindaraj A, Rao C. Bundles of aligned carbon nanotubes obtained by the pyrolysis of ferrocene–hydrocarbon mixtures: role of the metal nanoparticles produced in situ. Chem Phys Lett 1999;307:158–62.
[24] Popov VN. Carbon nanotubes: properties and application. Mater Sci Eng R Rep 2004;43:61–102.
[25] Shao Y, Yin G, Gao Y, Shi P. Durability study of Pt/C and Pt/CNTs catalysts under simulated PEM fuel cell conditions. J Electrochem Soc 2006;153:A1093–7.
[26] Kil KC, Hong SG, Park JO, Pak C, Chang H, Paik U. The use of MWCNT to enhance oxygen reduction reaction and adhesion strength between catalyst layer and gas diffusion layer in polymer electrolyte membrane fuel cell. Int J Hydrogen Energy 2014;39:17481–6.
[27] Beltrán-Gastélum M, Salazar-Gastelum MI, Felix-Navarro RM, Perez-Sicairos S, Reynoso-Soto EA, Lin SW, et al. Evaluation of Pt Au/MWCNT (multiwalled carbon nanotubes) electrocatalyst performance as cathode of a proton exchange membrane fuel cell. Energy 2016;109:446–55.
[28] Li W, Liang C, Zhou W, Qiu J, Zhou Z, Sun G, et al. Preparation and characterization of multiwalled carbon nanotube-supported platinum for cathode catalysts of direct methanol fuel cells. J Phys Chem B 2003;107:6292–9.
[29] Li W, Liang C, Qiu J, Zhou W, Han H, Wei Z, et al. Carbon nanotubes as support for cathode catalyst of a direct methanol fuel cell. Carbon 2002;40:791–4.
[30] Kongkanand A, Kuwabata S, Girishkumar G, Kamat P. Single-wall carbon nanotubes supported platinum nanoparticles with improved electrocatalytic activity for oxygen reduction reaction. Langmuir 2006;22:2392–6.
[31] Girishkumar G, Hall TD, Vinodgopal K, Kamat PV. Single wall carbon nanotube supports for portable direct methanol fuel cells. J Phys Chem B 2006;110:107–14.
[32] Lesiak B, Mazurkiewicz M, Malolepszy A, Stobinski L, Mierzwa B, Mikolajczuk-Zychora A, et al. Effect of the Pd/MWCNTs anode catalysts preparation methods on their morphology and activity in a direct formic acid fuel cell. Appl Surf Sci 2016;387:929–37.
[33] Shanmugam S, Gedanken A. Electrochemical properties of bamboo-shaped multiwalled carbon nanotubes generated by solid state pyrolysis. Electrochem Commun 2006;8:1099–105.
[34] Kurusu F, Tsunado H, Saito A, Tomita A, Kadota A, Kayahara N, et al. The advantage of using carbon nanotubes compared with edge plane pyrolytic graphite as an electrode material for oxidase-based biosensors. Analyst 2006;131:1292–8.
[35] Liu T, Liang R, Okoli O, Zhang M. Fabrication of silicon nanowire on freestanding multiwalled carbon nanotubes by chemical vapor deposition. Mater Lett 2015;159:353–6.
[36] Stankovich S, Dikin DA, Piner RD, Kohlhaas KA, Kleinhammes A, Jia Y, et al. Synthesis of graphene-based nanosheets via chemical reduction of exfoliated graphite oxide. Carbon 2007;45:1558–65.
[37] Chen Z, Higgins D, Chen Z. Nitrogen doped carbon nanotubes and their impact on the oxygen reduction reaction in fuel cells. Carbon 2010;48:3057–65.
[38] Zhang Y, Ge J, Wang L, Wang D, Ding F, Tao X, et al. Manageable N-doped graphene for high performance oxygen reduction reaction. Sci Rep 2013;3.

[39] Zhong G, Wang H, Yu H, Peng F. Nitrogen doped carbon nanotubes with encapsulated ferric carbide as excellent electrocatalyst for oxygen reduction reaction in acid and alkaline media. J Power Sources 2015;286:495–503.
[40] Sharifi T. Efficient electrocatalysts based on nitrogen-doped carbon nanostructures for energy applications. Umeå University; 2015.
[41] Zhuang Z, Giles SA, Zheng J, Jenness GR, Caratzoulas S, Vlachos DG. Nickel supported on nitrogen-doped carbon nanotubes as hydrogen oxidation reaction catalyst in alkaline electrolyte. Nat Commun 2016;7.
[42] La Torre Riveros L. Undoped and boron doped diamond nanoparticles as platinum and platinum-ruthenium catalyst support for direct methanol fuel cell application. 2010.
[43] La-Torre-Riveros L, Guzman-Blas R, Mendez-Torres AE, Prelas M, Tryk DA, Cabrera CR. Diamond nanoparticles as a support for Pt and PtRu catalysts for direct methanol fuel cells. ACS Appl Mater Interfaces 2012;4:1134–47.
[44] Brillas E, Huitle CAM. Synthetic diamond films: preparation, electrochemistry, characterization and applications, vol. 8. John Wiley & Sons; 2011.
[45] Salazar-Banda GR, Eguiluz KI, Avaca LA. Boron-doped diamond powder as catalyst support for fuel cell applications. Electrochem Commun 2007;9:59–64.
[46] Halima A, Rana U, MacFarlane D. Boron-doped diamond (BDD) coatings protect underlying silicon in aqueous acidic media—application to the hydrogen evolution reaction. Electrochim Acta 2014;115:639–43.
[47] Montilla F, Morallon E, Duo I, Comninellis CH, Vazquez JL. Platinum particles deposited on synthetic boron-doped diamond surfaces. Application to methanol oxidation. Electrochim Acta 2003;48:3891–7.
[48] Kim J, Chun YS, Lee SK, Lim DS. Improved electrode durability using a boron-doped diamond catalyst support for proton exchange membrane fuel cells. RSC Adv 2015;5:1103–8.
[49] Haenni W, Rychen P. In: Nebel Ch, editor. M. fryda and C. Comninellis in thin-film diamond part B. Academic Press, Semiconductors and Semimetals series, Elsevier; 2004.
[50] Kraft A. Doped diamond: a compact review on a new, versatile electrode material. Int J Electrochem Sci 2007;2:355–85.
[51] Lee B, Buchholz DB, Chang RP. An all carbon counter electrode for dye sensitized solar cells. Energy Environ Sci 2012;5:6941–52.
[52] Lu L, Xu H, Ren R, Zhao H. Graphite nanofibers as catalyst support for proton exchange membrane fuel cells at 80°C. In: 2010 Asia-Pacific power and energy engineering conference. IEEE; 2010.
[53] Abdullah MR, Rahmanifar MS, Hamedi F. Study of graphite addition on electrochemical activity of platinum on zinc oxide electrocatalyst for oxygen reduction reaction in pem fuel cell. 2013.
[54] Li YY, Li CT, Yeh MH, Huang KC, Chen PW, Vittal R, et al. Graphite with different structures as catalysts for counter electrodes in dye-sensitized solar cells. Electrochim Acta 2015;179:211–9.
[55] Wei YS, Jin QQ, Ren TZ. Expanded graphite/pencil-lead as counter electrode for dye-sensitized solar cells. Solid State Electron 2011;63:76–82.
[56] Wenmao T, Qun P, Yanyan L, Nan W. Microcrystalline graphite oxide as durable catalyst support for PEM fuel cell. Int J Electrochem Sci 2012;7:11578–87.
[57] Peera SG, Arunchander A, Sahu A. Platinum nanoparticles supported on nitrogen and fluorine co-doped graphite nanofibers as an excellent and durable oxygen reduction catalyst for polymer electrolyte fuel cells. Carbon 2016;107:667–79.
[58] Wang MX, Xu F, Sun HF, Liu Q, Artyushkova K, Stach EA, et al. Nanoscale graphite-supported Pt catalysts for oxygen reduction reactions in fuel cells. Electrochim Acta 2011;56:2566–73.
[59] Xiao M, Lu Y, Wang SJ, Zhao YF, Meng YZ. Poly (arylene disulfide)/graphite nanosheets composites as bipolar plates for polymer electrolyte membrane fuel cells. J Power Sources 2006;160:165–74.
[60] Hsieh CK, Tsai MC, Su CY, Wei SY, Yen MY, Ma CCM, et al. A hybrid nanostructure of platinum-nanoparticles/graphitic-nanofibers as a three-dimensional counter electrode in dye-sensitized solar cells. Chem Commun 2011;47:11528–30.
[61] Lee WJ, Ramasamy E, Lee DY, Song JS. Efficient dye-sensitized solar cells with catalytic multiwall carbon nanotube counter electrodes. ACS Appl Mater Interfaces 2009;1:1145–9.
[62] Seo SH, Kim SY, Koo BK, Cha SI, Lee DY. Influence of electrolyte composition on the photovoltaic performance and stability of dye-sensitized solar cells with multiwalled carbon nanotube catalysts. Langmuir 2010;26:10341–6.
[63] Zhang J, Long H, Miralles SG, Bisquert J, Fabregat-Santiago F, Zhang M. The combination of a polymer–carbon composite electrode with a high-absorptivity ruthenium dye achieves an efficient dye-sensitized solar cell based on a thiolate–disulfide redox couple. Phys Chem Chem Phys 2012;14:7131–6.
[64] Winther-Jensen B, Winther-Jensen O, Forsyth M, MacFarlane DR. High rates of oxygen reduction over a vapor phase–polymerized PEDOT electrode. Science 2008;321:671–4.
[65] Peramo A, Urbanchek MG, Spanninga SA, Povlich LK, Cederna P, Martin DC. In situ polymerization of a conductive polymer in acellular muscle tissue constructs. Tissue Eng Part A 2008;14:423–32.
[66] Zhang X, Pang S, Chen X, Zhang K, Liu Z, Zhou X, et al. An insight into the effect of nitrogen doping on the performance of a reduced graphene oxide counter electrode for dye-sensitized solar cells. RSC Adv 2013;3:9005–10.
[67] Mabena LF, Ray SS, Mhlanga SD, Coville NJ. Nitrogen-doped carbon nanotubes as a metal catalyst support. Appl Nanosci 2011;1:67–77.
[68] Strelko V, Kuts V, Thrower P. On the mechanism of possible influence of heteroatoms of nitrogen, boron and phosphorus in a carbon matrix on the catalytic activity of carbons in electron transfer reactions. Carbon 2000;38:1499–503.
[69] Strelko VV, Kartel NT, Dukhno IN, Kuts VS, Clarkson RB, Odintsov BM. Mechanism of reductive oxygen adsorption on active carbons with various surface chemistry. Surf Sci 2004;548:281–90.
[70] Ajayan P. Nanotubes from carbon. Chem Rev 1999;99:1787.
[71] Matter PH, Wang E, Ozkan US. Preparation of nanostructured nitrogen-containing carbon catalysts for the oxygen reduction reaction from SiO_2-and MgO-supported metal particles. J Catal 2006;243:395–403.
[72] Ghosh K, Kumar M, Maruyama T, Ando Y. Tailoring the field emission property of nitrogen-doped carbon nanotubes by controlling the graphitic/pyridinic substitution. Carbon 2010;48:191–200.
[73] Ma J, Li C, Yu F, Chen J. 3 D single-walled carbon nanotube/graphene aerogels as Pt-Free transparent counter electrodes for high efficiency dye-sensitized solar cells. ChemSusChem 2014;7:3304–11.
[74] Maitra T, Sharma S, Srivastava A, Cho YK, Madou M, Sharma A. Improved graphitization and electrical conductivity of suspended carbon nanofibers derived from carbon nanotube/polyacrylonitrile composites by directed electrospinning. Carbon 2012;50:1753–61.

[75] Geim AK, Novoselov KS. The rise of graphene. Nat Mater 2007;6:183–91.
[76] Geim AK. Graphene: status and prospects. Science 2009;324:1530–4.
[77] Antolini E. Graphene as a new carbon support for low-temperature fuel cell catalysts. Appl Catal B Environ 2012;123:52–68.
[78] Zhang G, Lu W, Cao F, Xiao Z, Zheng X. N-doped graphene coupled with Co nanoparticles as an efficient electrocatalyst for oxygen reduction in alkaline media. J Power Sources 2016;302:114–25.
[79] Jafri RI, Rajalakshmi N, Dhathathreyan KS, Ramaprabhu S. Nitrogen doped graphene prepared by hydrothermal and thermal solid state methods as catalyst supports for fuel cell. Int J Hydrogen Energy 2015;40:4337–48.
[80] Guo J, Wang R, Tjiu WW, Pan J, Liu T. Synthesis of Fe nanoparticles@ graphene composites for environmental applications. J Hazard Mater 2012;225:63–73.
[81] Kim B, Yu A, Chen Z. One step synthesis of iron deposited nitrogen doped graphene as a highly active electrocatalyst for oxygen reduction reaction. In: 223rd ECS meeting (May 12–17, 2013). Ecs; 2013.
[82] Chen M, Liu J, Zhou W, Lin J, Shen Z. Nitrogen-doped graphene-supported transition-metals carbide electrocatalysts for oxygen reduction reaction. Sci Rep 2015;5.
[83] Panchakarla L, Govindaraj A, Rao C. Boron-and nitrogen-doped carbon nanotubes and graphene. Inorg Chim Acta 2010;363:4163–74.
[84] Wang H, Maiyalagan T, Wang X. Review on recent progress in nitrogen-doped graphene: synthesis, characterization, and its potential applications. ACS Catal 2012;2:781–94.
[85] Yang Z, Yao Z, Li G, Fang G, Nie H, Liu Z, et al. Sulfur-doped graphene as an efficient metal-free cathode catalyst for oxygen reduction. ACS Nano 2011;6:205–11.
[86] Stoller MD, Park S, Zhu Y, An J, Ruoff RS. Graphene-based ultracapacitors. Nano Lett 2008;8:3498–502.
[87] Balandin AA. Thermal properties of graphene and nanostructured carbon materials. Nat Mater 2011;10:569–81.
[88] Pop E, Varshney V, Roy AK. Thermal properties of graphene: fundamentals and applications. MRS Bull 2012;37:1273–81.
[89] Marinho B, Ghislandi M, Tkalya E, Koning CE, de With G. Electrical conductivity of compacts of graphene, multi-wall carbon nanotubes, carbon black, and graphite powder. Powder Technol 2012;221:351–8.
[90] Neto AC, Guinea F, Peres NMR, Novoselov KS, Geim AK. The electronic properties of graphene. Rev Mod Phys 2009;81:109.
[91] Brownson DA, Kampouris DK, Banks CE. An overview of graphene in energy production and storage applications. J Power Sources 2011;196:4873–85.
[92] Choi HJ, Jung SM, Seo JM, Chang DW, Dai L, Baek JB. Graphene for energy conversion and storage in fuel cells and supercapacitors. Nano Energy 2012;1:534–51.
[93] Choi SM, Seo MH, Kim HJ, Kim WB. Synthesis of surface-functionalized graphene nanosheets with high Pt-loadings and their applications to methanol electrooxidation. Carbon 2011;9:904–9.
[94] Novoselov KS, Geim AK, Morozov SV, Jiang D, Zhang Y, Dubonos SV, et al. Electric field effect in atomically thin carbon films. Science 2004;306:666–9.
[95] Avouris P, Dimitrakopoulos C. Graphene: synthesis and applications. Mater Today 2012;15:86–97.
[96] Choucair M, Thordarson P, Stride JA. Gram-scale production of graphene based on solvothermal synthesis and sonication. Nat Nanotechnol 2009;4:30–3.
[97] Tripathi P, Patel CH, Prakash R, Shaz MA, Srivastava ON. Synthesis of high-quality graphene through electrochemical exfoliation of graphite in alkaline electrolyte. 2013. arXiv preprint arXiv:1310.7371.
[98] Stankovich S, Piner RD, Chen X, Wu N, Nguyen ST, Ruoff RS. Stable aqueous dispersions of graphitic nanoplatelets via the reduction of exfoliated graphite oxide in the presence of poly (sodium 4-styrenesulfonate). J Mater Chem 2006;16:155–8.
[99] Li Y, Tang L, Li J. Preparation and electrochemical performance for methanol oxidation of Pt/graphene nanocomposites. Electrochem Commun 2009;11:846–9.
[100] Seselj N, Engelbrekt C, Zhang J. Graphene-supported platinum catalysts for fuel cells. Sci Bull 2015;60:864–76.
[101] Park S, Shao Y, Wan H, Rieke PC, Viswanathan VV, Towne SA, et al. Design of graphene sheets-supported Pt catalyst layer in PEM fuel cells. Electrochem Commun 2011;13:258–61.
[102] Marinkas A, Arena F, Mitzel J, Prinz GM, Heinzel A, Peinecke V, et al. Graphene as catalyst support: the influences of carbon additives and catalyst preparation methods on the performance of PEM fuel cells. Carbon 2013;58:139–50.
[103] Yoo E, Okata T, Akita T, Kohyama M, Nakamura J, Honma I. Enhanced electrocatalytic activity of Pt subnanoclusters on graphene nanosheet surface. Nano Lett 2009;9:2255–9.
[104] Seger B, Kamat PV. Electrocatalytically active graphene-platinum nanocomposites. Role of 2-D carbon support in PEM fuel cells. J Phys Chem C 2009;113(19):7990–5.
[105] Zhou Y, Neyerlin K, Olson TS, Pylypenko S, Bult J, Dinh HN, et al. Enhancement of Pt and Pt-alloy fuel cell catalyst activity and durability via nitrogen-modified carbon supports. Energy Environ Sci 2010;3(10):1437–46.
[106] Subramanian NP, Li X, Nallathambi V, Kumaraguru SP, Colon-Mercado H, Wu G, et al. Nitrogen-modified carbon-based catalysts for oxygen reduction reaction in polymer electrolyte membrane fuel cells. J Power Sources 2009;188:38–44.
[107] Thirumal V, Pandurangan A, Jayavel R, Ilangovan R. Synthesis and characterization of boron doped graphene nanosheets for supercapacitor applications. Synth Met 2016;220:524–32.
[108] Agnoli S, Favaro M. Doping graphene with boron: a review of synthesis methods, physicochemical characterization, and emerging applications. J Mater Chem A 2016;4:5002–25.
[109] Chen Z, Higgins D, Chen Z. Electrocatalytic activity of nitrogen doped carbon nanotubes with different morphologies for oxygen reduction reaction. Electrochim Acta 2010;55:4799–804.
[110] Shi Q, Peng F, Liao S, Wang H, Yu H, Liu Z, et al. Sulfur and nitrogen co-doped carbon nanotubes for enhancing electrochemical oxygen reduction activity in acidic and alkaline media. J Mater Chem A 2013;1:14853–7.
[111] Raj CR, Samanta A, Noh SH, Mondal S, Okajima T, Ohsaka T. Emerging new generation electrocatalysts for the oxygen reduction reaction. J Mater Chem A 2016;4(29):11156–78.
[112] Zheng Y, Jiao Y, Jaroniec M, Jin Y, Qiao SZ. Nanostructured metal-free electrochemical catalysts for highly efficient oxygen reduction. Small 2012;8(23):3550–66.
[113] Ewels CP, Glerup M. Nitrogen doping in carbon nanotubes. J Nanosci Nanotechnol 2005;5(9):1345–63.
[114] Shao Y, Sui J, Yin G, Gao Y. Nitrogen-doped carbon nanostructures and their composites as catalytic materials for proton exchange membrane fuel cell. Appl Catal B Environ 2008;79(1):89–99.
[115] Droppa R, Hammer P, Carvalho ACM, Santos MC, Alvarez F. Incorporation of nitrogen in carbon nanotubes. J Non Cryst Solids 2002;299:874–9.

[116] Glerup M, Steinmetz J, Samaille D, Stephan O, Enouz S, Loiseau A, et al. Synthesis of N-doped SWNT using the arc-discharge procedure. Chem Phys Lett 2004;387(1):193–7.
[117] Hummelen JC, Knight BW, Pavlovich J, Gonzalez R, Wudl F. Isolation of the heterofullerene C59N as its dimer (C59N) 2. Science-New York then Washington; 1995. 1554–1554.
[118] Glenis S, Cooke S, Chen X, Labes MM. Photophysical properties of fullerenes prepared in an atmosphere of pyrrole. Chem Mater 1994;6(10):1850–3.
[119] Ying ZC, Hettich RL, Compton RN, Haufler RE. Synthesis of nitrogen-doped fullerenes by laser ablation. J Phys B Atom Mol Opt Phys 1996;29(21):4935.
[120] Maldonado S, Morin S, Stevenson KJ. Structure, composition, and chemical reactivity of carbon nanotubes by selective nitrogen doping. Carbon 2006;44:1429–37.
[121] Wang EG. A new development in covalently bonded carbon nitride and related materials. Adv Mater 1999;11(13):1129–33.
[122] Srivastava SK, Vankar VD, Rao DVS, Kumar V. Enhanced field emission characteristics of nitrogen-doped carbon nanotube films grown by microwave plasma enhanced chemical vapor deposition process. Thin Solid Films 2006;515(4):1851–6.
[123] Srivastava D, Menon M, Daraio C, Jin S, Sadanadan B, Rao AM. Vacancy-mediated mechanism of nitrogen substitution in carbon nanotubes. Phys Rev B 2004;69(15):153414.
[124] Koós AA, Dowling M, Jurkschat K, Crossley A, Grobert N. Effect of the experimental parameters on the structure of nitrogen-doped carbon nanotubes produced by aerosol chemical vapour deposition. Carbon 2009;47(1):30–7.
[125] Chen Y, Wang J, Liu H, Li R, Sun X, Ye S, et al. Enhanced stability of Pt electrocatalysts by nitrogen doping in CNTs for PEM fuel cells. Electrochem Commun 2009;11(10):2071–6.
[126] Zamudio A, Elias AL, Rodriguez-Manzo AJ, Lopez-Urias F, Rodriguez-Gattorno G, Lupo F, et al. Efficient anchoring of silver nanoparticles on N-Doped carbon nanotubes. Small 2006;2(3):346–50.
[127] Guo L, Jiang WJ, Zhang Y, Hu JS, Wei ZD, Wan LJ. Embedding Pt nanocrystals in N-doped porous carbon/carbon nanotubes toward highly stable electrocatalysts for the oxygen reduction reaction. ACS Catal 2015;5(5):2903–9.
[128] Qu L, Liu Y, Baek JB, Dai L. Nitrogen-doped graphene as efficient metal-free electrocatalyst for oxygen reduction in fuel cells. ACS Nano 2010;4(3):1321–6.
[129] Wu J, Pisula W, Müllen K. Graphenes as potential material for electronics. Chem Rev 2007;107(3):718–47.
[130] Casanovas J, Ricart JM, Rubio J, Illas F, Jimenez-Mateos JM. Origin of the large N 1s binding energy in X-ray photoelectron spectra of calcined carbonaceous materials. J Am Chem Soc 1996;118(34):8071–6.
[131] Wei D, Liu Y, Wang Y, Zhang H, Huang L, Yu G. Synthesis of N-doped graphene by chemical vapor deposition and its electrical properties. Nano Lett 2009;9(5):1752–8.
[132] Geng D, Yang S, Zhang Y, Yang J, Liu J, Li R, et al. Nitrogen doping effects on the structure of graphene. Appl Surf Sci 2011;257(21):9193–8.
[133] Vikkisk M, Kruusenberg I, Joost U, Shulga E, Kink I, Tammeveski K. Electrocatalytic oxygen reduction on nitrogen-doped graphene in alkaline media. Appl Catal B Environ 2014;147:369–76.
[134] Sheng ZH, Shao L, Chen JJ, Bao WJ, Wang FB, Xia XH. Catalyst-free synthesis of nitrogen-doped graphene via thermal annealing graphite oxide with melamine and its excellent electrocatalysis. ACS Nano 2011;5(6):4350–8.
[135] Jafri RI, Rajalakshmi N, Ramaprabhu S. Nitrogen doped graphene nanoplatelets as catalyst support for oxygen reduction reaction in proton exchange membrane fuel cell. J Mater Chem 2010;20(34):7114–7.
[136] Shao Y, Zhang S, Engelhard MH, Li G, Shao G, Wang Y, et al. Nitrogen-doped graphene and its electrochemical applications. J Mater Chem 2010;20(35):7491–6.
[137] Lepró X, Terres E, Vega-Cantu Y, Rodriguez-Macias FJ, Muramatsu H, Kim YA, et al. Efficient anchorage of Pt clusters on N-doped carbon nanotubes and their catalytic activity. Chem Phys Lett 2008;463(1):124–9.
[138] Groves MN, Chan ASW, Malardier-Jugroot C, Jugroot M. Improving platinum catalyst binding energy to graphene through nitrogen doping. Chem Phys Lette 2009;481(4):214–9.
[139] Maldonado S, Stevenson KJ. Influence of nitrogen doping on oxygen reduction electrocatalysis at carbon nanofiber electrodes. J Phys Chem B 2005;109(10):4707–16.
[140] Zhang LS, Liang XQ, Song WG, Wu ZY. Identification of the nitrogen species on N-doped graphene layers and Pt/NG composite catalyst for direct methanol fuel cell. Phys Chem Chem Phys 2010;12(38):12055–9.
[141] Xiong B, Zhou Y, Zhou Y, Wang J, Chen X, O'Hayre R, et al. The use of nitrogen-doped graphene supporting Pt nanoparticles as a catalyst for methanol electrocatalytic oxidation. Carbon 2013;52:181–92.
[142] Reddy ALM, Srivastava A, Gowda SR, Gullapalli H, Dubey M, Ajayan PM. Synthesis of nitrogen-doped graphene films for lithium battery application. ACS Nano 2010;4(11):6337–42.
[143] Wu G, Mack NH, Gao W, Ma S, Zhong R, Han J, et al. Nitrogen-doped graphene-rich catalysts derived from heteroatom polymers for oxygen reduction in nonaqueous lithium–O_2 battery cathodes. ACS Nano 2012;6(11):9764–76.
[144] Wang Y, Shao Y, Matson DW, Li J, Lin Y. Nitrogen-doped graphene and its application in electrochemical biosensing. ACS Nano 2010;4(4):1790–8.
[145] Kannan P, Maiyalagan T, Sahoo ND, Opallo M. Nitrogen doped graphene nanosheet supported platinum nanoparticles as high performance electrochemical homocysteine biosensors. J Mater Chem B 2013;1(36):4655–66.
[146] Kiciński W, Szala M, Bystrzejewski M. Sulfur-doped porous carbons: synthesis and applications. Carbon 2014;68:1–32.
[147] Terrones M, Souza Filho AG, Rao AM. Doped carbon nanotubes: synthesis, characterization and applications. In: Carbon nanotubes. Springer; 2007. p. 31–566.
[148] Sun Y, Du C, An M, Du L, Tan Q, Liu C, et al. Boron-doped graphene as promising support for platinum catalyst with superior activity towards the methanol electrooxidation reaction. J Power Sources 2015;300:245–53.
[149] Pullamsetty A, Subbiah M, Sundara R. Platinum on boron doped graphene as cathode electrocatalyst for proton exchange membrane fuel cells. Int J Hydrogen Energy 2015;40(32):10251–61.
[150] Chen YX, Miki A, Ye S, Sakai H, Osawa M. Formate, an active intermediate for direct oxidation of methanol on Pt electrode. J Am Chem Soc 2003;125(13):3680–1.
[151] Yang S, Zhi L, Tang K, Feng X, Maier J, Mullen K. Efficient synthesis of heteroatom (N or S)-doped graphene based on ultrathin graphene oxide-porous silica sheets for oxygen reduction reactions. Adv Funct Mater 2012;22(17):3634–40.
[152] Paraknowitsch JP, Thomas A. Doping carbons beyond nitrogen: an overview of advanced heteroatom doped carbons with boron, sulphur and phosphorus for energy applications. Energy Environ Sci 2013;6(10):2839–55.
[153] Li X, Wang H, Robinson JT, Sanchez H, Diankov G, Dai H. Simultaneous nitrogen doping and reduction of graphene oxide. J Am Chem Soc 2009;131(43):15939–44.
[154] Wang L, Jia W, Liu X, Li J, Titirici MM. Sulphur-doped ordered mesoporous carbon with enhanced electrocatalytic

activity for the oxygen reduction reaction. J Energy Chem 2016;25(4):566–70.
[155] Gao H, Liu Z, Song L, Guo W, Gao W, Ci L, et al. Synthesis of S-doped graphene by liquid precursor. Nanotechnol 2012;23(27):275605.
[156] Dai J, Yuan J, Giannozzi P. Gas adsorption on graphene doped with B, N, Al, and S: a theoretical study. Appl Phys Lett 2009;95(23):232105.
[157] Sheng ZH, Gao HL, Bao WJ, Wang FB, Xia XH. Synthesis of boron doped graphene for oxygen reduction reaction in fuel cells. J Mater Chem 2012;22(2):390–5.
[158] Park J-E, Jang YJ, Kim YJ, Song M-S, Yoon S, Kim DH, et al. Sulfur-doped graphene as a potential alternative metal-free electrocatalyst and Pt-catalyst supporting material for oxygen reduction reaction. Phys Chem Chem Phys 2014;16(1):103–9.
[159] Higgins D, Hoque MA, Seo MH, Wang R, Hassan F, Choi JY, et al. Development and simulation of sulfur-doped graphene supported platinum with exemplary stability and activity towards oxygen reduction. Adv Funct Mater 2014;24(27):4325–36.
[160] Wang R, Higgins DC, Hoque MA, Lee DU, Hassan F, Chen Z. Controlled growth of platinum nanowire arrays on sulfur doped graphene as high performance electrocatalyst. Sci Rep 2013;3.
[161] Xu C. Enhanced durability of Pt alloy nanoparticles using sulfur-doped graphene via metal-support interactions for PEMFC cathode catalysis of ORR. University of Waterloo; 2017.
[162] Denis PA, Faccio R, Mombru AW. Is it possible to dope single-walled carbon nanotubes and graphene with sulfur? ChemPhysChem 2009;10(4):715–22.
[163] Denis PA. When noncovalent interactions are stronger than covalent bonds: Bilayer graphene doped with second row atoms, aluminum, silicon, phosphorus and sulfur. Chem Phys Lett 2011;508(1):95–101.
[164] Denis PA. Concentration dependence of the band gaps of phosphorus and sulfur doped graphene. Comput Mater Sci 2013;67:203–6.
[165] Lv H, Mu S, Cheng N, Pan M. Nano-silicon carbide supported catalysts for PEM fuel cells with high electrochemical stability and improved performance by addition of carbon. Appl Catal B Environ 2010;100:190–6.
[166] Cui Y, Wei Q, Park H, Lieber CM. Nanowire nanosensors for highly sensitive and selective detection of biological and chemical species. Science 2001;293:1289–92.
[167] Von Kraemer S, Wikander K, Lindbergh G, Lundblad A, Palmqvist AEC. Evaluation of TiO_2 as catalyst support in Pt-TiO_2/C composite cathodes for the proton exchange membrane fuel cell. J Power Sources 2008;180:185–90.
[168] Vannice MA, Chao YL, Friedman RM. The preparation and use of high surface area silicon carbide catalyst supports. Appl Catal 1986;20:91–107.
[169] Zhang J, Liang Y, Zhou Q, Peng Y, Yang H. Enhancing electrochemical properties of silicon-graphite anodes by the introduction of cobalt for lithium-ion batteries. J Power Sources 2015;290:71–9.
[170] Avasarala B, Murray T, Li W, Haldar P. Titanium nitride nanoparticles based electrocatalysts for proton exchange membrane fuel cells. J Mater Chem 2009;19:1803–5.
[171] Huang SY, Ganesan P, Park S, Popov BN. Development of a titanium dioxide-supported platinum catalyst with ultrahigh stability for polymer electrolyte membrane fuel cell applications. J Am Chem Soc 2009;131:13898–9.
[172] Elezović NR, Babic BM, Radmilovic VR, Vracar LM, Krstajic NV. Novel Pt catalyst on ruthenium doped TiO_2 support for oxygen reduction reaction. Appl Catal B Environ 2013;140:206–12.
[173] Selvarani G, Maheswari S, Sridhar P, Pitchumani S, Shukla AK. A PEFC with Pt–TiO_2/C as oxygen-reduction catalyst. J Fuel Cell Sci Technol 2011;8(2). 021003.
[174] Antolini E. Iridium as catalyst and cocatalyst for oxygen evolution/reduction in acidic polymer electrolyte membrane electrolyzers and fuel cells. ACS Catal 2014;4(5):1426–40.
[175] Trasatti S. Physical electrochemistry of ceramic oxides. Electrochim Acta 1991;36(2):225–41.
[176] Suchsland J-P, Klose-Schubert B, Herein D, Martin T, Eickes C, Lennartz T. The potential of non carbon based catalysts for automotive fuel cells. ECS Trans 2013;50(2):1659–67.
[177] Binninger T, Fabbri E, Kotz R, Schmidt TJ. Iridium-titanium oxide as support for Pt catalyst in PEFC cathodes. ECS Trans 2013;58(1):1835–41.
[178] Cruz JC, Baglio V, Siracusano S, Ornelas R, Arriaga LG, Antonucci V, et al. Nanosized Pt/IrO_2 electrocatalyst prepared by modified polyol method for application as dual function oxygen electrode in unitized regenerative fuel cells. Int J Hydrogen Energy 2012;37(7):5508–17.
[179] Escalante-García I, Durron-Torres SM, Cruz JC, Arriaga-Hurtado LG. Electrochemical characterization of IrO_2-Pt and RuO_2-Pt mixtures as bifunctional electrodes for unitized regenerative fuel cells. J New Mat Electrochem Sys 2010;13:227–33.
[180] Zhang Y, Zhang H, Ma Y, Cheng J, Zhong H, Song S, et al. A novel bifunctional electrocatalyst for unitized regenerative fuel cell. J Power Sources 2010;195(1):142–5.
[181] Kong FD, Zhang S, Yin GP, Zhang N, Wang ZB, Du CY. Preparation of Pt/Irx (IrO_2) 10– x bifunctional oxygen catalyst for unitized regenerative fuel cell. J Power Sources 2012;210:321–6.
[182] Kong FD, Zhang S, Yin GP, Wang ZB, Du CY, Chen GY, et al. Electrochemical studies of Pt/Ir–IrO_2 electrocatalyst as a bifunctional oxygen electrode. Int J Hydrogen Energy 2012;37(1):59–67.
[183] Lori O, Elbaz L. Advances in ceramic supports for polymer electrolyte fuel cells. Catalysts 2015;5(3):1445–64.
[184] Zayim E, Mohseni AT. Structural and optical properties of tungsten oxide based thin films and nanofibers. Low-dimensional and nanostructured materials and devices. Springer; 2016. p. 291–307.
[185] Chhina H, Campbell S, Kesler O. Ex situ evaluation of tungsten oxide as a catalyst support for PEMFCs. J Electrochem Soc 2007;154(6):B533–9.
[186] Rajesh B, Karthik V, Karthikeyan S, Thampi KR, Bonard JM, Viswanathan B. Pt–WO_3 supported on carbon nanotubes as possible anodes for direct methanol fuel cells. Fuel 2002;81(17):2177–90.
[187] Muthuraman N, Guruvaiah PK, Agneeswara PG. High performance carbon supported Pt–WO_3 nanocomposite electrocatalysts for polymer electrolyte membrane fuel cell. Mater Chem Phys 2012;133(2–3):924–31.
[188] Mobarakeh MD. Synthesis of electrospun carbon nanofiber/WO_3 supported Pt, Pt/Pd and Pt/Ru catalysts for fuel cells. Fibers Polym 2017;18(1):95–101.
[189] Wu F, Liu Y, Wu C. Preparation and characterization of Pt-WO_3/C catalysts for direct ethanol fuel cells. Rare Met 2010;29(3):255–60.
[190] Zhang DY, Ma ZF, Wang G, Konstantinov K, Yuan X, Liu HK. Electro-oxidation of ethanol on Pt-WO_3/C electrocatalyst. Electrochem Solid State Lett 2006;9(9):A423–6.
[191] Nakada M, Ishihara A, Mitsushima S, Kamiya N, Ota K-I. Effect of tin oxides on oxide formation and reduction of platinum particles. Electrochem Solid State Lett 2007;10(1):F1–4.
[192] Okanishi T, Matsui T, Takeguchi T, Kikuchi R, Eguchi K. Chemical interaction between Pt and SnO_2 and influence on

adsorptive properties of carbon monoxide. Appl Catal A General 2006;298:181–7.
[193] Zhang P, Huang SY, Popov BN. Mesoporous tin oxide as an oxidation-resistant catalyst support for proton exchange membrane fuel cells. J Electrochem Soc 2010;157(8):B1163–72.
[194] Saha MS, Li R, Cai M, Sun X. High electrocatalytic activity of platinum nanoparticles on SnO_2 nanowire-based electrodes. Electrochem Solid State Lett 2007;10(8):B130–3.
[195] Dou M, Hou M, Liang D, Lu W, Shao Z, Yi B. SnO_2 nanocluster supported Pt catalyst with high stability for proton exchange membrane fuel cells. Electrochim Acta 2013;92:468–73.
[196] Qian Y, Ismail IM, Stein A. Ultralight, high-surface-area, multifunctional graphene-based aerogels from self-assembly of graphene oxide and resol. Carbon 2014;68:221–31.
[197] Klechikov A, Mercier G, Sharifi T, Baburin IA, Seifert G, Talyzin AV. Hydrogen storage in high surface area graphene scaffolds. Chem Commun 2015;51:15280–3.
[198] Peigney A, Laurent C, Flahaut E, Bacsa RR, Rousset A. Specific surface area of carbon nanotubes and bundles of carbon nanotubes. Carbon 2001;39:507–14.
[199] Li HQ, Wang YG, Wang CX, Xia YY. A competitive candidate material for aqueous supercapacitors: high surface-area graphite. J Power Sources 2008;185:1557–62.
[200] Swope V, Sasaki I, Ay A, Swain GM. Conductive diamond powder: a new catalyst support for the polymer electrolyte membrane fuel cell. ECS Trans 2007;3:27–36.
[201] Hao JY, Wang YY, Gong CW, Tian YM, Liang LP. Novel synthesis of high surface area SiC by carbothermal reduction process. Mater Res Innov 2015;19:155–9.
[202] Wang DH, Fu X. Synthesis of high surface area porous silicon carbide by employing soft template in the sol-gel process. In: Adv Mater Res. Trans Tech Publ.; 2011.
[203] Wang HY, Chen J, Hy S, Yu L, Xu Z, Liu B. High-surface-area mesoporous TiO_2 microspheres via one-step nanoparticle self-assembly for enhanced lithium-ion storage. Nanoscale 2014;6:14926–31.
[204] Song S, Zhang H, Ma X, Shao Z, Baker RT, Yi B. Electrochemical investigation of electrocatalysts for the oxygen evolution reaction in PEM water electrolyzers. Int J Hydrogen Energy 2008;33(19):4955–61.
[205] Vermaire D, Van Berge P. The preparation of tungsten oxide powders with high specific surface areas. J Mater Sci 1988;23(11):3963–9.
[206] Masuda Y, Ohji T, Kato K. Highly enhanced surface area of tin oxide nanocrystals. J Am Ceram Soc 2010;93(8):2140–3.
[207] Yano H, Watanabe M, Iiyama A, Uchida H. Particle-size effect of Pt cathode catalysts on durability in fuel cells. Nano Energy 2016;29:323–33.
[208] Xu Z, Zhang H, Zhong H, Lu Q, Wang Y, Su D. Effect of particle size on the activity and durability of the Pt/C electrocatalyst for proton exchange membrane fuel cells. Appl Catal B Environ 2012;111:264–70.
[209] Gummalla M, Ball SC, Condit DA, Rasouli S, Yu K, Ferreira PJ, et al. Effect of particle size and operating conditions on Pt3Co PEMFC cathode catalyst durability. Catalysts 2015;5:926–48.
[210] Ahluwalia RK, Arisetty S, Wang X, Wang X, Subbaraman R, Ball SC, et al. Thermodynamics and kinetics of platinum dissolution from carbon-supported electrocatalysts in aqueous media under potentiostatic and potentiodynamic conditions. J Electrochem Soc 2013;160:F447–55.
[211] Li D, Wang C, Strmcnik DS, Tripkovic DV, Sun X, Kang Y, et al. Functional links between Pt single crystal morphology and nanoparticles with different size and shape: the oxygen reduction reaction case. Energy Environ Sci 2014;7:4061–9.
[212] Park IS, Park KW, Choi JH, Park CR, Sung YE. Electrocatalytic enhancement of methanol oxidation by graphite nanofibers with a high loading of PtRu alloy nanoparticles. Carbon 2007;45(1):28–33.
[213] Matsutani K, Hayakawa K, Tada T. Effect of particle size of platinum and platinum-cobalt catalysts on stability against load cycling. Platin Met Rev 2010;54:223–32.
[214] Beyribey B, Corbacioğlu B, Altin Z. Synthesis of platinum particles from H_2PtCl_6 with hydrazine as reducing agent. Gazi Univ J Sci 2009;22(4):351–7.
[215] Verde Y, Alonso-Nunez G, Miki-Yoshida M, Jose-Yacaman M, Ramos VH, Keer A. Active area and particle size of Pt particles synthesized from (NH_4) $2PtCl_6$ on a carbon support. Catal Today 2005;107:826–30.
[216] Chen Y, Wang J, Liu H, Banis MN, Li R, Sun X, et al. Nitrogen doping effects on carbon nanotubes and the origin of the enhanced electrocatalytic activity of supported Pt for proton-exchange membrane fuel cells. J Phys Chem C 2011;115(9):3769–76.
[217] Wang X, Li W, Chen Z, Waje M, Yan Y. Durability investigation of carbon nanotube as catalyst support for proton exchange membrane fuel cell. J Power Sources 2006;158:154–9.
[218] Li Y, Gao W, Ci L, Wang C, Ajayan PM. Catalytic performance of Pt nanoparticles on reduced graphene oxide for methanol electro-oxidation. Carbon 2010;48(4):1124–30.
[219] Tsang K-Y, Lee T-C, Ren J, Chan K-Y, Wang H, Wang H. Platinum tungsten oxide (Pt–WO_3) nanoparticles: their preparation in glycol and electrocatalytic properties. J Exp Nanosci 2006;1(1):113–23.
[220] Hoque MA, Hassan FM, Higgins D, Choi J-Y, Pritzker M, Knights S, et al. Multigrain platinum nanowires consisting of oriented nanoparticles anchored on sulfur-doped graphene as a highly active and durable oxygen reduction electrocatalyst. Adv Mater 2015;27(7):1229–34.
[221] Singh R, Awasthi R, Sharma C. An overview of recent development of platinum-based cathode materials for direct methanol fuel cells. Int J Electrochem Sci 2014;9:5607–39.
[222] Kopke M, Held C, Hujer S, Liesegang H, Wiezer A, Wollherr A, et al. Clostridium ljungdahlii represents a microbial production platform based on syngas. Proc Natl Acad Sci 2010;107(29):13087–92.
[223] Lu Y, Jiang Y, Gao X, Chen W. Charge state-dependent catalytic activity of [Au 25 (SC 12 H 25) 18] nanoclusters for the two-electron reduction of dioxygen to hydrogen peroxide. Chem Commun 2014;50(62):8464–7.
[224] Pearce C, Lloyd J, Guthrie J. The removal of colour from textile wastewater using whole bacterial cells: a review. Dyes Pigment 2003;58(3):179–96.
[225] Song C, Zhang J. Electrocatalytic oxygen reduction reaction, in PEM fuel cell electrocatalysts and catalyst layers. Springer; 2008. p. 89–134.
[226] Mayrhofer KJJ, Strmcnik D, Blizanac BB, Stamenkovic V, Arenz M, Markovic NM. Measurement of oxygen reduction activities via the rotating disc electrode method: from Pt model surfaces to carbon-supported high surface area catalysts. Electrochim Acta 2008;53(7):3181–8.
[227] Mayrhofer KJJ, Blazanac BB, Arenz M, Stamenkovic VR, Ross PN, Markovic NM. The impact of geometric and surface electronic properties of Pt-catalysts on the particle size effect in electrocatalysis. J Phys Chem B 2005;109(30):14433–40.
[228] Sattler M, Ross P. The surface structure of Pt crystallites supported on carbon black. Ultramicroscopy 1986;20(1–2):21–8.
[229] Hwang JT, Chung JS. The morphological and surface properties and their relationship with oxygen reduction

activity for platinum-iron electrocatalysts. Electrochim Acta 1993;38(18):2715–23.
[230] Maillard F, Martin M, Gloaguen F, Leger J-M. Oxygen electroreduction on carbon-supported platinum catalysts. Particle-size effect on the tolerance to methanol competition. Electrochim Acta 2002;47(21):3431–40.
[231] Peuckert M, Yoneda T, Betta RAD, Boudart M. Oxygen reduction on small supported platinum particles. J Electrochem Soc 1986;133(5):944–7.
[232] Bing Y, Liu H, Zhang L, Ghosh D, Zhang J. Nanostructured Pt-alloy electrocatalysts for PEM fuel cell oxygen reduction reaction. Chem Soc Rev 2010;39(6):2184–202.
[233] Lee K, Zhang J, Wang H, Wilkinson DP. Progress in the synthesis of carbon nanotube-and nanofiber-supported Pt electrocatalysts for PEM fuel cell catalysis. J Appl Electrochem 2006;36(5):507–22.
[234] Sun KG, Chung JS, Hur SH. Durability improvement of Pt/RGO catalysts for PEMFC by low-temperature self-catalyzed reduction. Nanoscale Res Lett 2015;10(1):1.
[235] González-González I, Lorenzo-Medrano C, Cabrera CR. Sequential electrodeposition of platinum-ruthenium at boron-doped diamond electrodes for methanol oxidation. Adv Phys Chem 2011;2011, 679246.
[236] Ay A. Boron doped ultrananocrystalline diamond powder: alternative support material for PEMFCs. Michigan State University; 2011.
[237] Lyu X, Hu J, Foord JS, Lou C, Zhang W. Synthesis and electrocatalytic performance of BDD-supported platinum nanoparticles. J Mater Eng Perform 2015;24:1031–7.
[238] Siburian R. Support material effect for Pt catalytic activity at cathode. Int Res J Pure Appl Chem 2014;4:541.
[239] Xin Y, Liu JG, Zhou Y, Liu W, Gao J, Xie Y, et al. Preparation and characterization of Pt supported on graphene with enhanced electrocatalytic activity in fuel cell. J Power Sources 2011;196:1012–8.
[240] Kou R, Shao Y, Wang D, Engelhard MH, Kwak JH, Wang J, et al. Enhanced activity and stability of Pt catalysts on functionalized graphene sheets for electrocatalytic oxygen reduction. Electrochem Commun 2009;11:954–7.
[241] Fuentes RE, Colón-Mercado HR, Martínez-Rodríguez MJ. Pt-Ir/TiC electrocatalysts for PEM fuel cell/electrolyzer process. J Electrochem Soc 2014;161(1):F77–82.
[242] Zhang J, Tu J-P, Du G-H, Dong Z-M, Su Q-M, Xie D, et al. Pt supported self-assembled nest-like-porous WO_3 hierarchical microspheres as electrocatalyst for methanol oxidation. Electrochim Acta 2013;88:107–11.
[243] Masao A, Noda S, Takasaki F, Ito K, Sasaki K. Carbon-free Pt electrocatalysts supported on SnO_2 for polymer electrolyte fuel cells. Electrochem Solid State Lett 2009;12(9):B119–22.
[244] Debe MK. Electrocatalyst approaches and challenges for automotive fuel cells. Nature 2012;486:43.
[245] Gasteiger HA, Kocha SS, Sompalli B, Wagner FT. Activity benchmarks and requirements for Pt, Pt-alloy, and non-Pt oxygen reduction catalysts for PEMFCs. Appl Catal B Environ 2005;56:9–35.
[246] InvestmentMine. Historical platinum prices and price chart. 2017 [cited 2017 25 September]; Available from: http://www.infomine.com/investment/metal-prices/platinum/all/.
[247] Store, F.C.. Platinum black. 2017 [cited 2017 9 September 2017]; Available from: http://www.fuelcellstore.com/fuel-cell-components/catalyst/platinum-catalysts/platinum-black.
[248] Store, F.C. Platinum on carbon. 2017 [cited 2017 9 September]; Available from: http://www.fuelcellstore.com/80-platinum-carbon.
[249] Alfa Aesar, T.F.S. Platinum black, HiSPEC 1000. 2017 [cited 2017 9 September]; Available from: https://www.alfa.com/en/catalog/012755/.
[250] Sigma-Aldrich. Platinum black. 2017 [cited 2017 9 September]; Available from: http://www.sigmaaldrich.com/catalog/product/aldrich/520780?lang=en&region=MY.
[251] The Lab Depot, I. Platinum black. 2017 [cited 2017 9 September]; Available from: http://www.labdepotinc.com/p-21301-platinum-black-powder.php.
[252] Store, F.C. 50% platinum on carbon. 2017 [cited 2017 9 September]; Available from: http://www.fuelcellstore.com/50-platinum-carbon.
[253] Store, F.C. 10% platinum on carbon. 2017 [cited 2017 9 September]; Available from: http://www.fuelcellstore.com/10-platinum-carbon.
[254] Alfa Aesar, T.F.S. 10% platinum on carbon, HiSPEC 2000. 2017 [cited 2017 9 September]; Available from: https://www.alfa.com/en/catalog/043876/.
[255] Sigma-Aldrich. 10% platinum on carbon. 2017 [cited 2017 9 September]; Available from: http://www.sigmaaldrich.com/catalog/product/aldrich/738581?lang=en&region=MY&cm_sp=Insite-_-prodRecCold_xviews-_-prodRecCold10-7.
[256] Store, F.C. Platinum palladium black. 2017 [cited 2017 9 September]; Available from: http://www.fuelcellstore.com/fuel-cell-components/catalyst/platinum-catalysts/pt-alloy-catalysts/platinum-palladium-black.
[257] Alfa Aesar, T.F.S. 50% platinum palladium black, HiSPEC 6000. 2017 [cited 2017 9 September]; Available from: https://www.alfa.com/en/catalog/041171/.
[258] Store, F.C. 20% platinum palladium on vulcan. 2017 [cited 2017 9 September]; Available from: http://www.fuelcellstore.com/20-platinum-palladium-vulcan.
[259] Alfa Aesar, T.F.S. 40% platinum, 20% ruthenium on carbon black, HiSPEC 10000. 2017 [cited 2017 9 September]; Available from: https://www.alfa.com/en/catalog/044172/.
[260] Store, F.C. 20% platinum nickel on vulcan. 2017 [cited 2017 9 September]; Available from: http://www.fuelcellstore.com/20-platinum-nickel-vulcan.
[261] Store, F.C. 20% platinum ruthenium on vulcan. 2017 [cited 2017 9 September]; Available from: http://www.fuelcellstore.com/20-platinum-ruthenium.
[262] Store, F.C. 20% platinum copper on vulcan. 2017 [cited 2017 9 September]; Available from: http://www.fuelcellstore.com/20-platinum-copper-vulcan.
[263] Store, F.C. 20% platinum tin on vulcan. 2017 [cited 2017 9 September]; Available from: http://www.fuelcellstore.com/20-platinum-tin-vulcan.
[264] Store, F.C. 20% platinum iridium on vulcan. 2017 [cited 2017 9 September]; Available from: http://www.fuelcellstore.com/20-platinum-iridium-vulcan.
[265] Store, F.C. 20% platinum cobalt on vulcan. 2017 [cited 2017 9 September]; Available from: http://www.fuelcellstore.com/20-platinum-cobalt-vulcan.
[266] Store, F.C. Palladium black, high surface area. 2017 [cited 2017 9 September]; Available from: http://www.fuelcellstore.com/palladium-black-high-surface-area.
[267] The Lab Depot, I. Palladium black. 2017 [cited 2017 9 September]; Available from: http://www.labdepotinc.com/p-20694-palladium-black.php.
[268] Alfa Aesar, T.F.S. Palladium black. 2017 [cited 2017 9 September]; Available from: https://www.alfa.com/en/catalog/000659/.
[269] Store, F.C. Ruthenium black. 2017 [cited 2017 9 September]; Available from: http://www.fuelcellstore.com/ruthenium-black-high-surface-area.
[270] Store, F.C. 20% palladium on vulcan. 2017 [cited 2017 9 September]; Available from: http://www.fuelcellstore.com/20-palladium-vulcan.
[271] Store, F.C. 20% ruthenium on vulcan. 2017 [cited 2017 9 September]; Available from: http://www.fuelcellstore.com/ruthenium-20-vulcan.

[272] The Lab Depot, I. 5% ruthenium on carbon. 2017 [cited 2017 9 September]; Available from: http://www.labdepotinc.com/p-22129-ruthenium-5-on-carbon.php.
[273] Store, F.C. 20% gold on vulcan. 2017 [cited 2017 9 September]; Available from: http://www.fuelcellstore.com/20-gold-vulcan-standard.
[274] Store, F.C. 20% iron on vulcan. 2017 [cited 2017 9 September]; Available from: http://www.fuelcellstore.com/20-iron-vulcan?search=iron.
[275] Alia SM, Jensen K, Contreras C, Garzon F, Pivovar B, Yan Y. Platinum coated copper nanowires and platinum nanotubes as oxygen reduction electrocatalysts. ACS Catal 2013;3:358–62.
[276] Sorsa O, Romar H, Lassi U, Kallio T. Co-electrodeposited mesoporous PtM (M = Co, Ni, Cu) as an active catalyst for oxygen reduction reaction in a polymer electrolyte membrane fuel cell. Electrochim Acta 2017;230:49–57.
[277] Xu JB, Zhao TS, Yang WW, Shen SY. Effect of surface composition of Pt-Au alloy cathode catalyst on the performance of direct methanol fuel cells. Int J Hydrogen Energy 2010;35:8699–706.
[278] Li W, Zhou W, Li H, Zhou Z, Zhou B, Sun G, et al. Nano-structured Pt–Fe/C as cathode catalyst in direct methanol fuel cell. Electrochim Acta 2004;49:1045–55.
[279] Xiong L, Kannan A, Manthiram A. Pt–M (M = Fe, Co, Ni and Cu) electrocatalysts synthesized by an aqueous route for proton exchange membrane fuel cells. Electrochem Commun 2002;4:898–903.
[280] Tamaki T, Minagawa A, Arumugam B, Kakade BA, Yamaguchi T. Highly active and durable chemically ordered Pt–Fe–Co intermetallics as cathode catalysts of membrane–electrode assemblies in polymer electrolyte fuel cells. J Power Sources 2014;271:346–53.
[281] Zeng Y, Shao Z, Zhang H, Wang Z, Hong S, Yu H, et al. Nanostructured ultrathin catalyst layer based on open-walled PtCo bimetallic nanotube arrays for proton exchange membrane fuel cells. Nano Energy 2017;34:344–55.
[282] Hsin YL, Hwang KC, Yeh CT. Poly (vinylpyrrolidone)-modified graphite carbon nanofibers as promising supports for PtRu catalysts in direct methanol fuel cells. J Am Chem Soc 2007;129:9999–10010.
[283] Hyun K, Lee JH, Yoon CW, Kwon Y. The effect of platinum based bimetallic electrocatalysts on oxygen reduction reaction of proton exchange membrane fuel cells. Int J Electrochem Sci 2013;8:11752–67.
[284] Shi X, Iqbal N, Kunwar SS, Wahab G, Kasat HA, Kannan AM. Pt Co@ NCNTs cathode catalyst using ZIF-67 for proton exchange membrane fuel cell. Int J Hydrogen Energy 2017;43(6):3520–6.
[285] Cheng Y, Xu C, Shen PK, Jiang SP. Effect of nitrogen-containing functionalization on the electrocatalytic activity of PtRu nanoparticles supported on carbon nanotubes for direct methanol fuel cells. Appl Catal B Environ 2014;158:140–9.
[286] Jung WS, Popov BN. Improved durability of Pt catalyst supported on N-doped mesoporous graphitized carbon for oxygen reduction reaction in polymer electrolyte membrane fuel cells. Carbon 2017;122:746–55.
[287] Ozaki JI, Anahara T, Kimura N, Oya A. Simultaneous doping of boron and nitrogen into a carbon to enhance its oxygen reduction activity in proton exchange membrane fuel cells. Carbon 2006;44:3358–61.
[288] Antolini E. Platinum-based ternary catalysts for low temperature fuel cells: part I. Preparation methods and structural characteristics. Appl Catal B Environ 2007;74:324–36.
[289] Huang H, Wang X. Recent progress on carbon-based support materials for electrocatalysts of direct methanol fuel cells. J Mater Chem A 2014;2:6266–91.
[290] Salgado J, Antolini E, Gonzalez E. Preparation of Pt-Co/C electrocatalysts by reduction with borohydride in acid and alkaline media: the effect on the performance of the catalyst. J Power Sources 2004;138:56–60.
[291] Fernández JL, Raghuveer V, Manthiram A, Bard AJ. Pd– Ti and Pd– Co– Au electrocatalysts as a replacement for platinum for oxygen reduction in proton exchange membrane fuel cells. J Am Chem Soc 2005;127:13100–1.
[292] Feng Y, He T, Alonso-Vante N. Carbon-supported $CoSe_2$ nanoparticles for oxygen reduction reaction in acid medium. Fuel Cells 2010;10:77–83.
[293] Zhang G, Shao ZG, Lu W, Li G, Liu F, Yi B. One-pot synthesis of Ir@ Pt nanodendrites as highly active bifunctional electrocatalysts for oxygen reduction and oxygen evolution in acidic medium. Electrochem Commun 2012;22:145–8.
[294] Vinayan BP, Nagar R, Rajalakshmi N, Ramaprabhu S. Novel platinum–cobalt alloy nanoparticles dispersed on nitrogen-doped graphene as a cathode electrocatalyst for PEMFC applications. Adv Funct Mater 2012;22:3519–26.
[295] Kim HS, Lee Y, Lee JG, Hwang HJ, Jang J, Juon SM, et al. Platinum catalysts protected by N-doped carbon for highly efficient and durable polymer-electrolyte membrane fuel cells. Electrochim Acta 2016;193:191–8.
[296] Yang HN, Lee WH, Choi BS, Ko YD, Yi SC, Kim WJ. Self-humidifying Pt-C/Pt-TiO_2 dual-catalyst electrode membrane assembly for proton-exchange membrane fuel cells. Energy 2017;120:12–9.
[297] Dong L, Gari RRS, Li Z, Craig MM, Hou S. Graphene-supported platinum and platinum–ruthenium nanoparticles with high electrocatalytic activity for methanol and ethanol oxidation. Carbon 2010;48:781–7.
[298] Guo S, Sun S. FePt nanoparticles assembled on graphene as enhanced catalyst for oxygen reduction reaction. J Am Chem Soc 2012;134:2492–5.
[299] Liu CW, Chen HS, Lai CM, Lin JN, Tsai LD, Wang KW. Promotion of oxygen reduction reaction durability of carbon-supported PtAu catalysts by surface segregation and TiO_2 addition. ACS Appl Mater Interfaces 2014;6:1589–94.
[300] Park KW, Seol KS. Nb-TiO_2 supported Pt cathode catalyst for polymer electrolyte membrane fuel cells. Electrochem Commun 2007;9:2256–60.
[301] Ehrenfreund P, Foing BH. Fullerenes and cosmic carbon. Science 2010;329:1159–60.